

DESI and other dark energy experiments in the era of neutrino mass measurements

Andreu Font-Ribera^{a,1,2} Patrick McDonald,^{2,†} Nick Mostek,³ Beth A. Reid,² Hee-Jong Seo,² and Anže Slosar⁴

¹*Institute of Theoretical Physics, University of Zurich,
Winterthurerstrasse 190, 8057 Zurich, Switzerland*

²*Lawrence Berkeley National Laboratory, 1 Cyclotron Road, Berkeley, CA 94720, USA*

³*Space Sciences Laboratory, University of California, Berkeley, CA 94720, USA*

⁴*Brookhaven National Laboratory, Upton, NY 11973, USA*

(Dated: March 2, 2022)

We present Fisher matrix projections for future cosmological parameter measurements, including neutrino masses, dark energy, curvature, modified gravity, the inflationary perturbation spectrum, non-Gaussianity, and dark radiation. We focus on DESI and generally redshift surveys (BOSS, HETDEX, eBOSS, Euclid, and WFIRST), but also include CMB (Planck) and weak gravitational lensing (DES and LSST) constraints. The goal is to present a consistent set of projections, for concrete experiments, which are otherwise scattered throughout many papers and proposals. We include neutrino mass as a free parameter in most projections, as it will inevitably be relevant – DESI and other experiments can measure the sum of neutrino masses to ~ 0.02 eV or better, while the minimum possible sum is ~ 0.06 eV. We note that the BAO-only use of galaxy clustering is substantially degraded as a dark energy probe in the presence of neutrino mass uncertainty – using broadband galaxy power is critical, especially pushing it to as small a scale as possible, and big gains are achieved by combining lensing survey constraints with redshift survey constraints. We do not try to be especially innovative, e.g., in careful treatments of potential systematic errors – these projections are intended as a straightforward baseline for comparison to more detailed analyses.

I. INTRODUCTION

The Fisher matrix formalism is a standard tool for forecasting the statistical ability of future experiments to measure cosmological parameters of interest [1–10]. The Fisher matrix is the expectation value of the second derivative matrix of log likelihood with respect to parameters of interest

$$F_{AB} = - \left\langle \frac{\partial^2 \ln L}{\partial A \partial B} \right\rangle, \quad (1)$$

where L is likelihood, A and B are parameters and the average is over all possible realizations of the data assuming a certain fiducial model. In the limit of Gaussian likelihood, the Fisher information matrix can be thought of as the inverse of a typical covariance matrix. In particular, in the limit of Gaussian likelihood surface, $F_{AA}^{-1/2}$ is the expected error on the parameter A assuming the values of all other parameters are known, while $\sigma(A) = (F^{-1})_{AA}^{1/2}$ is the marginalized error on the parameter A . The Cramér-Rao bound also stipulates that no unbiased estimator of A performs better than the Fisher matrix error $\sigma(A)$ and therefore Fisher information is the lower limit on the error obtainable from a given data set using an optimal estimator.

Fisher matrix forecasts generally should not be taken literally for poorly constrained parameters where the likelihood will often be non-Gaussian [11–14], but even then the sense that the constraint is poor is generally preserved. When used thoughtfully, Fisher matrices allow us to map out the progression of parameter measurements we can expect from future experiments. Unfortunately, results of these exercises are generally scattered throughout the literature (or worse, non-public proposals), often with slightly different assumptions and methodologies that make direct comparisons difficult. The main purpose of this paper is make predictions for a suite of models and planned experiments with a consistent set of assumptions.

We do not attempt to be particularly innovative, but one thing we emphasize is that our basic cosmological model assumes that the neutrino mass is not known. Since the effect of massive neutrinos is important given the accuracy of the data we consider and since it is unlikely that it will be measured in terrestrial experiments in the next decade, it is a logical necessity to include it as a free parameter in all forecasts.

We also note that the Fisher formalism can never give an unambiguously fair comparison of experiments as it is impossible to anticipate and model all possible sources of systematic errors (see e.g. [15, 16]). It is also difficult to

^a author list alphabetized

[†] PVMcDonald@lbl.gov

forecast our advances in theoretical problems in the next decade (for example, our understanding of non-linear matter clustering, redshift-space distortions and biasing of cosmic tracers for the large scale structure probes; similar issues exist for all other probes). Therefore, we sometimes give pessimistic and optimistic forecasts (e.g., quoting BAO-only errors for a galaxy redshift survey is essentially a very pessimistic use of the survey).

The rest of this paper is structured as follows: In §II we define our cosmological parameters and fiducial model, and discuss general methodology. In §III we discuss our Cosmic Microwave Background, i.e., Planck, treatment. In §IV we discuss spectroscopic, i.e., redshift surveys like DESI. In §V we discuss photometric, i.e., gravitational lensing-oriented surveys. In §VI we give the main results on parameter constraints. Finally in §VII we give some discussion and conclusions. (In the Appendix we give some more traditional FoM numbers without free neutrino mass, and discuss the issue of overlapping lensing and redshift surveys.)

This is intended to be a technical reference paper – see, e.g., [10] for a much higher ratio of pedagogy to tables.

II. PARAMETERS, FIDUCIAL MODEL AND GENERAL METHODOLOGY

Our baseline model is flat Λ CDM with massive neutrinos. This model is specified by eight parameters which are listed, together with their fiducial values, in Table I. Parameter symbols have their conventional meanings. Capital Ω s are densities of various components expressed as a fraction of critical density today. Small case ω s correspond to physical density $\omega_x = \Omega_x h^2$ (for the component x), where h is the dimensionless reduced Hubble's parameter today $h = H_0/(100\text{km s}^{-1}\text{Mpc}^{-1})$. Matter density contains contribution from baryons, dark matter and massive neutrinos

$$\omega_m = \omega_b + \omega_{\text{cdm}} + \omega_\nu \quad (2)$$

(this is used only where massive neutrinos are non-relativistic). Parameter θ_s is angular size of sound horizon at the surface of last scattering, i.e.

$$\theta_s = r(a_\star)^{-1} s, \quad (3)$$

where

$$s = \int_0^{t_\star} \frac{c_s(t)}{a} dt = \int_0^{a_\star} \frac{c_s(a)}{a^2 H(a)} da. \quad (4)$$

Here c_s is the sound speed of cosmic plasma, r is the comoving angular diameter distance and a_\star is the scale factor at the redshift of decoupling as given in a fitting formula in [17].

Our standard fiducial parameter values follow Planck results, specifically the P+WP+highL+BAO column of Table 5 of [18]. As mentioned before, in addition to the conventional 6 parameters of the minimal cosmological model, we also always vary the neutrino mass and the amount of tensor modes. Varying neutrino mass is crucial in order to avoid biases in the parameter estimation, even before the neutrino mass is formally detected. Varying T/S is largely irrelevant to anything else in the paper because the T/S measurement is completely dominated by Planck and essentially uncorrelated with anything else – the error is always $\sigma_{T/S} = 0.006$, so we do not print it in tables.

Our modified gravity model is similar to but not exactly that of [19]. Rather than defining $d \ln D / d \ln a = \Omega_m^\gamma$ with γ as a free parameter, we define $d \ln D / d \ln a = f_{\text{GR}}(a) \Omega_m^{\Delta\gamma}$, where $\Delta\gamma$ is the free parameter, with a fiducial value of zero, and $f_{\text{GR}}(a)$ is $d \ln D / d \ln a$ computed given the background evolution and assuming GR. This is of course exactly equivalent to the usual parameterization if f_{GR} is exactly described by Ω_m^γ with unvarying γ , but allows for any variation in γ within GR to be properly propagated (we originally implemented this form because neutrinos certainly modify γ in principle, but in practice it did not make a noticeable difference – note that with neutrinos Ω_m here is defined to only include CDM and baryons). Similarly following [19], we include a parameter representing a multiplicative offset of the amplitude of perturbations, G_9 ([19] called it G_0), relative to the GR-predicted amplitude at $z = 9$ (applied to the $z < 9$ power, to decouple the low redshift amplitude from CMB measurements), i.e., for every use of the power spectrum other than the CMB, we multiply it by G_9^2 (as pointed out by [20], Eq. (29) of [19] and the text that follows it could be interpreted as defining G_9 in a way that deviated from 1 even within GR – clearly this would be a bad thing, although the definition of parameters list at the start of §III of [19] suggests that they really intended the definition to be the one we are using here, which does not have this problem).

Through this work we assume Gaussian likelihoods and propagate experimental designs into the Fisher matrices for the intermediate products of individual experiments, such as Fisher matrices for power spectrum measurements, or BAO distance scale parameters. These intermediate results are in turn used to form Fisher matrices for cosmological parameters for individual experiments. Except as otherwise discussed, we assume experimental errors are independent and combine experiments by adding their Fisher matrices.

TABLE I. Parameterization of the cosmological model and parameter values for the fiducial model. See text for discussion of symbol meanings. Eight parameters in the upper part of the table are always free. Parameters in the second half of the table are extensions of the simplest model discussed below.

Parameter	Value	Description
ω_b	0.02214	Physical baryon density $\omega_b = \Omega_b h^2$
ω_m	0.1414	Physical matter density $\omega_m = \Omega_m h^2$ (including neutrinos which are non-relativistic at $z = 0$)
θ_s	0.59680 degrees	Angular size of sound horizon at the surface of last scattering acting as a proxy for Hubble's constant
Σm_ν	0.06 eV	Sum of neutrino masses (we assume they are degenerate)
A_s	2.198×10^{-9}	Amplitude of the primordial power spectrum at $k = 0.05 \text{ Mpc}^{-1}$ (for the numerical Fisher matrix we actually use $\log_{10} A_s$)
n_s	0.9608	Spectral index of primordial matter fluctuations with $P(k) \propto k^{n_s}$
τ	0.092	Optical depth to the last scattering surface assuming instantaneous reionization.
T/S	0	Ratio of tensor to scalar perturbations (we assume inflationary tensor fluctuation's spectral index $n_t = -\frac{1}{8}T/S$)
w_0	-1	Equation of state of dark-energy $p = w\rho$
w'	0	Variable equation of state of dark energy of the form $w = w_0 + (1 - a)w'$
Ω_k	0	Curvature of the homogeneous model
$\Delta\gamma$	0	Modification of the growth factor $d \ln D / d \ln a = f_{\text{GR}}(a) \Omega_m(a)^{\Delta\gamma}$
G_9	1	Arbitrary normalization multiplier applied to the linear perturbations at $z < 9$, i.e., all our observables except the CMB.
α_s	0	Running of the spectral index $\alpha_s = d \log n_s / d \log k$ with pivot scale $k = 0.05 \text{ Mpc}^{-1}$
N_ν	3.04	Effective number of neutrino species ($N_\nu > 3.04 \rightarrow$ dark radiation).

For a typical vector of measured quantities, \mathbf{O} , for which we can assume the likelihood function is Gaussian, with vector of means, $\mathbf{O}(\theta)$, that is predictable given parameters θ , and covariance \mathbf{C} which we can assume is independent of the parameters, the Fisher matrix is:

$$F_{ij} = \frac{\partial \bar{\mathbf{O}}^T}{\partial \theta_i} \mathbf{C}^{-1} \frac{\partial \bar{\mathbf{O}}}{\partial \theta_j}. \quad (5)$$

The predictions for the linear perturbations in cosmological models are performed using CMBFAST [21], for historical reasons, but we have checked that results using CAMB [22] are virtually identical.

III. COSMIC MICROWAVE BACKGROUND: PLANCK

We include the Planck CMB satellite as a baseline experiment in all projections. Without it our interpretation of low redshift measurements would be dominated by constraints on strongly degenerate directions that are actually irrelevant in global constraints. Planck constraints are expected to improve with future releases including polarization, so we continue to project results using a Fisher matrix, following, e.g., [23]. We assume a usable fraction of the sky $f_{\text{sky}} = 0.7$. We assume 3 channels can be effectively used for cosmological measurements, 100, 143, and 217 GHz, with resolution 9.65, 7.25, and 4.99 arcmin, temperature noise 2.5, 2.2, and 4.8×10^{-6} per resolution element (in units of the mean temperature), and polarization noise 6.7, 4.0, and 9.8×10^{-6} [24]. We use all ℓ up to 2000 for temperature and 2500 for polarization. For equivalent parameter spaces, our Planck projections agree well with, e.g., [25–28].

IV. SPECTROSCOPIC SURVEYS

In this section we first describe how we compute projections for redshift surveys, including galaxy clustering, quasar clustering, and correlations of Ly α forest absorption in quasar spectra. Then we describe the specific redshift surveys we include.

A. Galaxy and quasar clustering

Galaxies and quasars are point tracers of the underlying cosmic structure. The physics of how they trace the dark matter fluctuations is well understood based on arguments about locality of galaxy formation [29–31] and heuristic understanding that astrophysical objects form in the peaks (halos) of the primordial density fields [32]. On very large scales bias is scale independent and redshift-space distortions are described by linear perturbation theory [33]. Beyond-linear perturbative corrections can be used on intermediate scales before perturbation theory breaks down entirely on small scales [34–44].

The basic model for galaxy clustering (or quasar clustering – when quasars are treated as clustering objects, as opposed to probes of the Ly α forest, there is no fundamental difference between them and galaxies) is simply linear bias and a shot noise contribution, i.e., $P_{ij}(k, \mu) = (b_i + f\mu^2)(b_j + f\mu^2)P_{\text{mass}}(k) + \bar{n}_i^{-1}\delta_{ij}^K$, where b_i is the bias for tracer type i , f is the growth rate, i.e., $f \equiv d \ln D / d \ln a$, μ is the cosine of the angle between the wavevector and our line of sight, $P_{\text{mass}}(k)$ is the linear theory mass power spectrum, and \bar{n} is the number density. We generally assume fiducial biases follow constant $b(z)D(z)$, where $D(z)$ is the linear growth factor normalized by $D(z=0) \equiv 1$.

1. BAO

Isolating the BAO feature gives the most robust, but pessimistic, view of the information that one can recover from galaxy clustering measurements, since BAO can be measured even in the presence of large unknown systematic effects (very generally these will not change the BAO scale [45]). Our treatment of isolated galaxy BAO follows [46], assuming 50% reconstruction, i.e., reduction of the BAO damping scale of [46] by a factor 0.5, except at very low number density, where we degrade reconstruction based on [47]. This method has held up well under close scrutiny [48–50]. We generally quote errors on the transverse and radial BAO scales as errors on $D_A(z)/s$ and $H(z)s$, respectively, where s is the BAO length scale. For galaxy and quasar clustering these errors always have nearly identical correlation coefficient 0.4. We also quote errors on an isotropic dilation factor R/s , defined as the error one would measure on a single parameter that rescales radial and transverse directions by equal amounts. Note that this is *not* equivalent to an error on $(D_A^2 H^{-1})^{1/3}$, as is easy to see by considering that, e.g., if we make a purely radial or purely transverse measurement, our fractional error on R/s is simply equal to the fractional error on Hs or D_A/s , while the error on $(D_A^2 H^{-1})^{1/3}$ is formally infinite, because one of the two parts is unconstrained ($(D_A^2 H^{-1})^{1/3}$ would be directly measured by something that was really sensitive to volume, e.g., counts of a source with known physical number density).

2. Broadband

Going beyond BAO, we use “broadband” galaxy power, i.e. measurements of the power spectrum as a function of redshift, wavenumber and angle with respect to the line of sight. This treatment automatically recovers all available information, i.e. not just the shape of the isotropic power spectrum, but also redshift-space distortions, Alcock-Paczynski [51], and of course also the BAO information. Discussing isolated redshift-space distortions as is often done, or the monopole power spectrum alone (which may sometimes be used for neutrino mass constraints), may be useful for pedagogical reasons, but generally once we go beyond BAO there is no clear systematic advantage in any subset of the broadband information, so it makes sense to just use all of it.

Bias uncertainty is modeled by a free parameter in each redshift bin, generally of width $\Delta z = 0.1$, for each type of galaxy. Our results are not sensitive to the redshift bin width, maybe surprisingly. For example, we show an explicit comparison of some cases in Table XXVII, and have checked other cases (e.g., the neutrino mass constraints we show are identical to two significant digits between $\Delta z = 0.1$ and $\Delta z = 0.2$ bins). We believe the reason for this is that the extra freedom allowed by, say, splitting an already fairly narrow bin in half, i.e., for the bias in one half to go up while the bias in the other goes down, still summing to what would have been the bias for the coarser bin, is not generally at all degenerate with cosmological parameters, because cosmological models generally do not predict this kind of rapid, anti-correlated change in relevant quantities like $f(z)$.

The broadband Fisher matrix is calculated by first computing the covariance matrix for $P_{ij}(k_{\parallel}, k_{\perp})$ given the noise and volume of each redshift slice in each survey, using

$$\langle (P_{ij} - \bar{P}_{ij}) (P_{mn} - \bar{P}_{mn}) \rangle = \frac{2\pi^2}{Vk^2 \Delta k \Delta \mu} (P_{im} P_{jn} + P_{in} P_{jm}) , \quad (6)$$

where V is the volume of the survey and Δk and $\Delta \mu$ are the bin widths (this formula is really only correct in the small-bin limit, and in practice we make the bins fine enough that the Fisher calculation is effectively an integral –

note that as defined here that integral only covers $0 < \mu < 1$). Then Eq. 5 is evaluated by taking numerical derivatives of $P_{ij}(k_{\parallel}, k_{\perp})$ with respect to all parameters, where $P_{ij}(k_{\parallel}, k_{\perp})$ is in observable coordinates (i.e., km s^{-1} and degrees).

We use broadband power up to some quoted $k_{\text{max,eff}}$. At $k > k_{\text{max,eff}}$ we continue to use BAO information as usual (to be clear, we compute the usual BAO fisher matrix, but cut modes with $k < k_{\text{max,eff}}$ out of the integration, since they are already included in the broadband calculation). We use two simple choices of $k_{\text{max,eff}}$, 0.1 and 0.2 $h\text{Mpc}^{-1}$. These should not be taken literally as a scale up to which we think linear theory will be sufficient for an analysis of future high precision data. Deviations will clearly be present even at 0.1 $h\text{Mpc}^{-1}$. These cutoffs are just intended to give an idea of the sensitivity of results to the effective scale where information is recovered after making corrections for non-linearity, presumably including some marginalization over beyond-linear bias parameters (information at higher k might be used to constrain these parameters – this is why we write $k_{\text{max,eff}}$, where “eff” stands for “effective”, instead of simply k_{max}). It will be a major program of the next decade to figure out exactly how to do this fitting in practice for a high precision survey like DESI – how well we can do this will determine how well we can measure parameters. The value 0.1-0.2 $h\text{Mpc}^{-1}$ is motivated by, e.g., the finding of [52] that a Taylor series representation of redshift space distortions could be summed to high precision up to $k \sim 0.2 h\text{Mpc}^{-1}$, after which it appeared that the power spectrum had become deeply non-linear, i.e., information is probably hopelessly scrambled, and many other similar findings (e.g., [40–42, 53–56]).

As an additional measure to be sure we are not making unreasonable predictions using the non-linear regime, we use the same information damping factors from [46] that we use for BAO for the broadband signal. This is well-motivated from a theoretical point of view, i.e., the damping is essentially the propagator of [57], which suppresses all linear theory information, not just BAO. We also include the reconstruction factor (50% reduction in damping length), as there is no logical reason why similar methods could not be used to recover non-BAO information, although this has not been worked through yet. The logic for also using $k_{\text{max,eff}}$ for broadband power (i.e., not relying on these damping factors as our only cutoff), and only using BAO beyond that, is that, while for BAO we largely only need to worry about the statistical effect of damping the signal relative to effective noise power coming from higher order terms, to use the broadband power this effective noise must actually be predicted, which is generally harder. To reiterate: the damping factors are applied as an additional limitation on the higher k power spectrum, in addition to $k_{\text{max,eff}}$, and the reconstruction factor is included to make the broadband treatment consistent with the isolated BAO treatment (i.e., note that if we did not do this the BAO information at $k < k_{\text{max,eff}}$ would not be the same between isolated BAO and broadband cases, which clearly does not make sense, although we could in principle adjust it as an additional step).

3. Isolated redshift-space distortions

Frequently, galaxy constraints beyond BAO are described as a measurement of a single redshift-space distortion (RSD) amplitude as a function of z , e.g., “ $f(z)\sigma_8(z)$ ”. While it is always nice to have a one dimensional scalar function to make simple plots, we do not use this method for our main results because it requires us to either ignore or marginalize away the uncertainty in geometry and the primordial power spectrum shape. It is easy enough, although harder to visualize, to just include all of the broadband information. However, since it has come to be expected, we do quote isolated RSD errors as a function of redshift for BOSS and DESI, calculated as described in [58]. This calculation makes the assumption that both the geometry and power spectrum shape are fixed by external constraints. This is probably the only scenario in which an isolated RSD measurement is a useful thing to quote, but we do not claim it applies in our cases. Specifically, if we assume the k -dependence of $P_{\text{mass}}(k)$ is known, the formula $P_{\text{red}}(k, \mu) = (b + f\mu^2)^2 P_{\text{mass}}(k)$ decomposes into a function of two parameters, $b\sigma$ and $f\sigma$, where $\sigma(z) \propto P_{\text{mass}}^{1/2}(z, k)$ is the rms normalization of the linear mass density fluctuations as a function of z . In tables, we identify the maximum k used to compute the error on $f\sigma$ by labeling it $f\sigma_k$, e.g., $f\sigma_{0.1}$ means the error calculation included information up to $k_{\text{max,eff}} = 0.1 h\text{Mpc}^{-1}$. These fractional errors are equivalent to what one usually sees quoted as an error on “ $f\sigma_8$ ”, i.e., σ_8 here is intended only loosely as a parameter normalizing the power spectrum, not to mean that you necessarily have a direct measurement of fluctuations on the scale of $8 h^{-1}\text{Mpc}$ radius spheres. We need to make the scale of sensitivity more explicit, because we have more than one. As in the broadband case, we always include the information damping factors of [46], with reconstruction.

B. Ly α

Spectroscopic surveys designed for galaxy redshift surveys can often also probe large-scale structure using the Ly α forest [59, 60], i.e., the Lyman- α absorption by neutral gas in the intergalactic medium in the spectra of high redshift quasars (or maybe at faint enough magnitudes Lyman-break galaxies [61]).

We model the three dimensional power spectrum of Ly α fluctuations using the analytic formula of [62]:

$$P_F(k, \mu, z) = b_F(z)^2(1 + \beta_F(z)\mu^2)^2 P_{mass}(k, z) D(k, \mu, z), \quad (7)$$

where b_F is the linear bias parameter, β_F the redshift space distortion parameter and $D(k, \mu, z)$ is a non-linear correction calibrated from simulations. Table I of [62] gives parameter dependence of b_F , β_F , and fitting parameters of D .

Similar to galaxies, the Ly α forest can be viewed pessimistically as a probe of the BAO feature, or more optimistically using the broadband and smaller scale power spectrum.

1. BAO

The BAO distance scale has recently been measured in the three dimensional correlation of the Ly α forest in nearby quasar lines of sight from the BOSS survey [63, 64]. Using one third of the final BOSS area, the authors were able to measure BAO distance scale at redshift $z = 2.4$ with an uncertainty of 2% [64].

The parameters of Eq. 7 given by [62] are only valid near $z \sim 2.25$. For BAO error estimates, which we want to make well away from this redshift and do not require us to use detailed parameter dependence, we simply use the central model parameters (the Planck model happens to have nearly exactly the same amplitude and slope of the power spectrum relevant to the Ly α forest, although the WMAP model was lower) with the power spectrum additionally multiplied by a factor $((1+z)/3.2)^{3.8}$ to match the evolution of the 1D power with redshift [59]. Except as otherwise noted, we use the method of [61] to estimate the obtainable errors (a similar method was derived by [65]).

In contrast to past projections which often used the rest wavelength range $1041 < \lambda < 1185\text{\AA}$ (following [59]), we expand the range to include the Ly β forest and move slightly closer to the quasar, $985 < \lambda < 1200\text{\AA}$, reflecting our increasing confidence that we understand the relevant issues well enough to measure BAO across this range [66]. Gains from this enhancement of effective number density (and cross-correlations with quasars below) are substantial because the measurement is quite sparse, i.e., in what for galaxies we would call the shot-noise limited regime.

We isolate the BAO signal by subtracting a smoothed version of the power spectrum from the wiggly one and then using the residual wiggles in our Fisher matrix derivatives. We follow the procedure of [46] in dividing the noise contribution to the power errors by the $(1 + \beta\mu^2)^2$ RSD factor rather than including this factor in the derivative term, which would lead to artificial (i.e., non-BAO-distance) breaking of the degeneracy between radial and transverse distance errors (this was not done in [61], leading to some underestimation of the degeneracy between $H(z)$ and $D_A(z)$). We also include the [46] damping factors, with no reconstruction. We have tested that our approach agrees with [46] to percent level given matching assumed data sets. To be clear, the primary difference between the Ly α forest BAO Fisher matrix calculation and the galaxy version is the need to evaluate the equations in [61], integrating over the quasar luminosity function and spectrograph noise distribution to determine the signal to noise level as a function of redshift, with another difference being that we compute the error on BAO distance through direct Fisher matrix derivatives of the wiggles-only power spectrum rather than the procedure of [46] of averaging over a cosine squared approximation for the derivatives (but again, we have checked that these methods agree remarkably precisely).

2. Broadband and 1D power

The correlation of Ly α absorption in quasar spectra can provide other cosmological information beyond BAO. Several studies have already constrained cosmological parameters from the line of sight power spectrum [59, 67–75], and one can also obtain valuable information from the full shape of the three-dimensional clustering [62]. In the projections below we distinguish between Ly α forest BAO measurements and broadband measurements that include the one dimensional power spectrum measurement.

For interpreting broadband measurements, we need the parameter dependence of Table I of [62], i.e., b_F and β_F , along with the fitting parameters of $D(k, \mu)$, depend on the amplitude and slope of the linear power spectrum, temperature-density relation [76, 77], and mean level of absorption [78], all of which are varied in our Fisher matrix calculations. To help constrain these parameters, we include the 1D power spectrum that could be measured from ~ 100 (existing) high resolution spectra [79, 80].

The constraints from the Ly α forest are difficult to predict accurately, because they require careful simulation work to achieve [81–84] – more careful than the community had been able to muster so far. The numbers we give are intended to be a good central value guess, i.e., while there is uncertainty, it is at least as likely that we could do better as worse, basically because we intentionally leave a lot of information for “contingency.” For these projections we

TABLE II. Basic numbers for BOSS. $P_{0.2,0} \equiv P(k = 0.2 \text{ hMpc}^{-1}, \mu = 0)$, $P_{0.14,0.6} \equiv P(k = 0.14 \text{ hMpc}^{-1}, \mu = 0.6)$. $f(z)\sigma_k(z)$ is what is often called $f(z)\sigma_s(z)$ – more precisely, $\frac{\sigma_{f\sigma_k}}{f\sigma_k}$ is the fractional error on the normalization of $f(z)P^{1/2}(k, z)$, assuming known shape of the power spectrum and known geometry, using $k_{\text{max,eff}} = k \text{ hMpc}^{-1}$.

z	$\frac{\sigma_{DA/s}}{DA/s}$	$\frac{\sigma_{H_s}}{H_s}$	$\frac{\sigma_{R/s}}{R/s}$	$\bar{n}P_{0.2,0}$	$\bar{n}P_{0.14,0.6}$	V	$\frac{dN_{LRG}}{dz \text{ ddeg}^2}$	$\frac{\sigma_{f\sigma_{0.1}}}{f\sigma_{0.1}}$	$\frac{\sigma_{f\sigma_{0.2}}}{f\sigma_{0.2}}$
	%	%	%			$(h^{-1}\text{Gpc})^3$		%	%
0.05	10.64	19.44	7.34	1.79	4.08	0.03	8	49.99	24.75
0.15	4.07	7.46	2.81	1.81	4.16	0.16	50	18.88	9.25
0.25	2.53	4.64	1.75	1.83	4.24	0.40	125	11.68	5.66
0.35	1.86	3.42	1.29	1.86	4.32	0.70	222	8.64	4.13
0.45	1.50	2.74	1.03	1.88	4.38	1.04	332	7.02	3.32
0.55	1.27	2.32	0.88	1.90	4.43	1.39	447	6.06	2.84
0.65	1.60	2.68	1.07	0.71	1.65	1.73	208	6.23	3.30
0.75	6.00	9.01	3.87	0.09	0.20	2.05	30	13.73	10.42

continue to use the rest wavelength range $1041 < \lambda < 1185\text{\AA}$, although the Ly β forest region should provide valuable complementary information. We do not include the bispectrum or any other statistics besides the power spectrum, which are known to be powerful for breaking IGM model degeneracies (e.g., [85, 86]). We do not use cross-correlations with quasar density. Finally, we only use the redshift range 2-2.7. The original reason for this was the limited range of applicability of the parameters of [62], but it has the effect of reserving the large amount of higher redshift information to help allow for expansion in the modeling uncertainty.

C. Ly α F-quasar cross-correlation

The cross-correlation of quasars with the Ly α forest [87] provides a complementary measurement of BAO at high redshift. We use a high-noise approximation to combine separately computed constraints from Ly α forest and quasars into one. In general, if we have multiple observable tracers, o_i , of the mass density field, δ_m , of the form $o_i = c_i\delta_m + \epsilon_i$ where c_i is the generalized bias (including the RSD factor) and ϵ_i is the noise for tracer i where $\langle |\epsilon_i|^2 \rangle \equiv N_i$, and we assume the noise is uncorrelated (a generally good but not always perfect assumption [88–90]), it is easy to show that the optimally weighted estimate of δ_m has noise variance $(\sum_i c_i^2 N_i^{-1})^{-1}$, where this applies mode-by-mode in Fourier space. This is equivalent, for galaxies where $N_i = \bar{n}_i^{-1}$, to the statement that we can simply add $\bar{n}_i P_i$ to find the signal-to-noise ratio for the optimal combined tracer, where $P_i \equiv c_i^2 P_m$ (this is actually how we do our ELG, LRG, QSO combined BAO calculation, including full k and μ dependence). The rms fractional error on a combined BAO measurement can then be approximated by $\sigma_{\text{BAO}} = \sigma_{\text{BAO},V} \left[1 + (\sum_i P_i N_i^{-1})^{-1} \right]$ where $\sigma_{\text{BAO},V}$ is the fractional error we would find from the given volume in the zero noise limit and $P_i(k, \mu) N_i^{-1}(k, \mu)$ is evaluated at the typical k and μ of the BAO feature (remember that for the Ly α forest N does depend on $k_{\parallel} \equiv k\mu$). If we have BAO measurements from the individual tracers, which obey $\sigma_{\text{BAO},i} = \sigma_{\text{BAO},V} \left[1 + N_i P_i^{-1} \right]$, we can re-write $P_i N_i^{-1}$ in terms of $\sigma_{\text{BAO},i}$ and in the high noise limit obtain $\sigma_{\text{BAO}} \stackrel{N/S \rightarrow \infty}{=} \left(\sum_i \sigma_{\text{BAO},i}^{-1} \right)^{-1}$, i.e., the combined fractional BAO error is given by the inverse sum of individual fractional BAO errors, not by the inverse quadrature sum as it would be for measurements in different volumes (the same approach could be used to derive the error without the high noise approximation, it would just produce a more complicated-looking equation). This inverse sum property makes the addition of a subdominant tracer like the quasars surprisingly valuable, compared to our usual intuition based on inverse quadrature sums.

We will justify the high noise approximation for DESI below. It is certainly possible to do a full multiple-tracer Fisher matrix calculation for Ly α forest and quasars, like we do for ELG, LRG, and QSO tracers at lower redshift, but this approximation should be sufficient and is easier given the available code. We use cross-correlations with quasars only for BAO measurements, not for broadband, although generally they should add information there too.

D. BOSS

BOSS [91] is a 10000 sq. deg. survey that is almost completed. Analyzers have chosen a certain redshift binning for the data [92], but we give the continuous numbers we have been using for Fisher matrix projections in Table II.

We use $b_{\text{LRG}}(z)D(z) = 1.7$. For the Ly α forest calculations we use the luminosity function of [93], for magnitude $g < 22$, multiplied by 0.73, in order to match the observed number density of quasars [64].

The published analyses of the first BOSS data release (DR9) [92, 94] give us the opportunity to evaluate the Fisher matrix projections relative to achieved reality, which we do in the next two subsections, for BAO and RSD. DR9 covered an effective area of 3275 square degrees and these analyses focused only on the high redshift sample, CMASS, which dominates the redshift distribution above $z \sim 0.45$; the formal redshift cuts were $0.43 < z < 0.7$ and did not include any LOWZ targets. The number densities were very similar to our assumption (by design). [92] found clustering amplitude corresponding to $b\sigma_8(z = 0.57) = 1.23$, or $b(z = 0.57) = 1.97$ for our model with $\sigma_8(z = 0.57) = 0.624$, corresponding to $b(z)D(z) = 1.48$, in contrast to 1.7 that we assume in the Fisher matrix calculations.

1. BOSS BAO projections vs. reality

To match the CMASS sample presented in [94], we combine the three redshift bins in Table II at $z = 0.45, 0.55$, and 0.65 , halving the volume for $z = 0.45$ to account for the observed redshift range of $0.43 < z < 0.7$ (with much-suppressed number density at the low z end). We combine the errors by simply taking the inverse of the square root of the sum of inverse squares of fractional errors. The combined errors are rescaled to account for the effective area of 3275 square degrees. For the dilation factor, R/s , this gives projections of 1.85% error without reconstruction and 1.08% with reconstruction for the DR9 CMASS sample. Using the bias measured from the data as mentioned above, $bD = 1.48$, instead of $bD = 1.7$, and a slightly more exact match to the number density distribution, we derive 1.94% and 1.15%. This is to be compared with the average of the mocks in Fig. 13 of [94], which is approximately 2.6% and 1.8% before and after reconstruction, respectively, and therefore the mock results in [94] are 1.34 (before reconstruction) and 1.57 (after reconstruction) times the Fisher matrix projections. The actual measured results from the data are better than expected, 1.7% both before and after reconstruction, but if we believe the mocks accurately represent the statistics of the measurement these differences must be just statistical fluctuations, and in any case the post-reconstruction ratio of error measured from data to Fisher estimate is still 1.48.

We can only speculate about the reasons for this discrepancy, i.e., $\sim 34\%$ before reconstruction and $\sim 57\%$ after reconstruction. First, [94] used a spherically averaged power spectrum while our Fisher matrix assumes an anisotropic power spectrum when deriving an isotropic error. According to [95] (their eq. [9]), using a spherically averaged power spectrum would return a slightly worse error than using an anisotropic power spectrum and then projecting two dimensional errors in D_A/s and Hs on R/s ; for the fiducial value of f , we only expect $\sim 7\%$ difference in error. A non-Gaussian aspect could exist in a likelihood curve of the dilation factor in the real survey, however [94] estimates the likelihood to be fairly Gaussian. Meanwhile we expect that the sample variance on the errors of the dilation scale from the finite number of mocks is not big enough to explain this discrepancy; we expect $\sim 3\%$ for the 600 mocks (i.e., $1/\sqrt{600 \times 2}$). The level of a Finger-of-God in the CMASS sample introduces only a small effect in the Fisher errors and therefore cannot explain the $\sim 34\%$ discrepancy. It is possible that small scale power due to nonlinear structure growth and bias could have increased an effective shot noise level relative to the underlying BAO signal, although an amount of power large enough to increase the errors this much should be obvious in the band-power measurement. Finally, the power spectrum/correlation function estimators used in [94] are not precisely optimal, although we would not expect the effect to be this large.

The discrepancy between CMASS DR9 and the Fisher formalism increases after reconstruction. We note that the Fisher matrix errors have not been as rigorously tested for the reconstructed field as the original field (although see [49], which did do careful tests with a reconstructed field, although only for the mass density). The dependence of the noise properties of the reconstructed field on the details of the reconstruction needs detailed tests in the future. For example, the reconstruction in [92, 94] adapted conventions to restore isotropy on large scales, which were not used in many of the tests of the method, and may not have well understood noise properties.

We note that the geometry of DR9 was significantly stripey, i.e., not a nice compact (e.g., square) 3275 sq. deg. [94], which could lead to an unavoidable degradation in the measurement relative to the Fisher matrix, could degrade reconstruction, and could exacerbate any sub-optimality in the analysis. The next generation of analyses will be quite compact, so it will be interesting to see if the discrepancy is reduced.

The bottom line is: the errors predicted by BOSS collaboration mocks in [94] are significantly larger than standard Fisher matrix projections for them, and we haven't thought of anything that seems likely to explain this, considering the many tests that have been done. There are three logical possibilities that should be explored: the Fisher projections are overly optimistic somehow, the analysis of the mocks and data is significantly sub-optimal, or some flaw in the mocks leads to even a near-optimal analysis producing incorrectly large errors.

2. BOSS redshift-space distortion projections vs. reality

Predictions for RSD are generally less certain than for BAO (really we only project a range of possibilities, for different $k_{\text{max,eff}}$), but it is still useful to see how they compare to the real analysis of [92]. From Table II, we estimate the expected fractional error on $f\sigma_{0.1}$ ($f\sigma_{0.2}$) to be 4.0 (2.0)% for 10000 sq. deg., or 7.0 (3.4)% for DR9.

Model 2 in [92], which treats $f\sigma_8$ as a free parameter and marginalizes over uncertainty in the linear matter power spectrum and flat Λ CDM distance-redshift relation, finds $f\sigma_8 = 0.415 \pm 0.033$, which is an 8.0% fractional error (note that there is some statistical error in this kind of percent error, of order the error itself, e.g., this error of 0.033 is only 6.9% of our fiducial $f\sigma_8 = 0.48$). Table 2 of [92] shows that the uncertainty remaining after including CMB constraints on the linear matter power spectrum or Λ CDM distance-redshift relation does not contribute to the DR9 error budget for measuring $f\sigma_8$, so we can directly compare with the Fisher projections above. Table 2 of [92] also shows that the uncertainty would be reduced to 7.0% (6.0% of our fiducial value) if a Finger-of-God nuisance parameter were held fixed. Since the DR9 analysis was performed in configuration space and the Fisher analysis in Fourier space, an attempt to compare at equal k_{max} can only be approximate. [96] found an approximate mapping between minimum configuration scale s_{min} and an equivalent k_{max} , which suggests for the DR9 analysis $k_{\text{max}} \sim 0.14 \text{ hMpc}^{-1}$. The bottom line seems to be that the DR9 results are consistent with the projections assuming $k_{\text{max,eff}} \sim 0.1 \text{ hMpc}^{-1}$. This is consistent with the idea that fits will go to somewhat larger k than $k_{\text{max,eff}}$, but lose some information to marginalization over nuisance parameters describing nonlinear effects such as Fingers-of-God, and some to non-Gaussian errors that enhance the data covariance matrix above the naive Fisher prediction. We conclude that the scheme adopted in this work gives a reasonable estimate of constraints that are achievable today with $k_{\text{max,eff}} = 0.1$; we are optimistic that future theoretical improvements will further enhance the constraining power of future surveys.

E. eBOSS

eBOSS is a proposed extension of BOSS that would cover 7500 sq. deg., 6000 sq. deg. focused entirely on quasars and LRGs at slightly higher redshift than BOSS LRGs, and another 1500 sq. deg. that adds ELGs similar to those discussed below for DESI. Table III shows basic numbers for eBOSS [97]. eBOSS will also target quasars at $z > 2.15$ over the 7500 sq. deg., and re-observe some BOSS quasars to obtain better signal-to-noise in the spectra, in order to improve the Ly α BAO measurement from BOSS by $\sim 25\%$. For simplicity, we do not consider the Ly α part of eBOSS in our analysis.

We assume that we can add the constraints from the two areas as if they are independent (in the usual way of this kind of Fisher matrix, this will be correct up to survey edge effects).

F. HETDEX

For HETDEX (<http://hetdex.org>), we do not have a complete redshift distribution, only the number 0.8 million galaxies, area 420 sq. deg., and a redshift range $1.9 < z < 3.5$ [98], so we use a fixed $\frac{dN}{dz \text{ ddeg}^2} = 1190$. We use bias $b(z)D(z) = 0.89$ [98]. Table IV shows the basic HETDEX numbers.

In the interest of limiting the length of our main results tables, we only include a limited set of cases using HETDEX.

G. DESI

DESI (short for Dark Energy Spectroscopic Instrument [99]) is a galaxy and quasar redshift survey likely to run on the Mayall 4 meter telescope at Kitt Peak National Observatory near Tucson, AZ, over an approximately five year period from 2018 to 2022. The baseline area is 14000 sq. deg.. We also consider the possibility that the spectrograph could then be moved to the twin Blanco telescope in Chile to cover another ~ 10000 sq. deg. (it may also be possible to cover more than 14000 sq. deg. from the North). We take the BigBOSS numbers to represent DESI, although this is not set in stone (see [100, 101], but the numbers we actually use are revised ones presented in [99, 102]). DESI will target 3 types of objects: Luminous Red Galaxies (LRGs) are bright, highly biased red objects that are easy to target from spectroscopic data (since the galaxy target selection for BOSS is not exactly the same as for the SDSS I and II LRGs, they are distinguished as CMASS and LOWZ galaxies in BOSS analysis papers; however, at the level of this paper they are essentially the same class of objects, which we will call LRGs). A second class of objects are Emission Line Galaxies (ELGs) [103], which require a higher resolution spectrograph to type and redshift, since this is only possible if the OII doublet is resolved. ELGs are considerably less biased than LRGs. For ELGs we

TABLE III. Basic numbers for eBOSS. The redshift range is covered twice, first showing the 1500 sq. deg. that will include ELGs, and then the 6000 sq. deg. that will not.

z	$\frac{\sigma_{DA/s}}{DA/s}$	$\frac{\sigma_{Hs}}{Hs}$	$\frac{\sigma_{R/s}}{R/s}$	$\bar{n}P_{0.2,0}$	$\bar{n}P_{0.14,0.6}$	V	$\frac{dN_{ELG}}{dz d\text{deg}^2}$	$\frac{dN_{LRG}}{dz d\text{deg}^2}$	$\frac{dN_{QSO}}{dz d\text{deg}^2}$
	%	%	%			$(h^{-1}\text{Gpc})^3$			
0.55	32.45	48.38	20.91	0.05	0.11	0.21	0	11	0
0.65	3.63	6.15	2.44	0.95	2.28	0.26	156	240	0
0.75	3.42	5.53	2.26	0.83	2.17	0.31	619	139	0
0.85	4.02	6.09	2.59	0.50	1.32	0.35	506	76	0
0.95	10.60	13.71	6.40	0.11	0.29	0.39	159	8	0
1.05	21.65	29.28	13.39	0.05	0.11	0.43	0	0	44
1.15	22.11	29.85	13.67	0.04	0.10	0.46	0	0	44
1.25	19.07	25.83	11.80	0.05	0.12	0.49	0	0	53
1.35	19.30	26.14	11.95	0.05	0.11	0.51	0	0	53
1.45	16.98	23.06	10.53	0.05	0.12	0.53	0	0	62
1.55	17.09	23.23	10.60	0.05	0.12	0.55	0	0	62
1.65	18.46	25.07	11.45	0.04	0.10	0.57	0	0	57
1.75	18.52	25.19	11.50	0.04	0.10	0.58	0	0	57
1.85	20.09	27.32	12.47	0.04	0.09	0.59	0	0	52
1.95	20.11	27.39	12.49	0.04	0.09	0.60	0	0	52
2.05	21.94	29.90	13.64	0.03	0.08	0.60	0	0	47
2.15	21.93	29.93	13.64	0.03	0.08	0.61	0	0	47
0.55	16.22	24.19	10.45	0.05	0.11	0.83	0	11	0
0.65	1.94	3.28	1.30	0.82	1.90	1.04	0	240	0
0.75	2.52	4.02	1.66	0.40	0.93	1.23	0	139	0
0.85	3.76	5.73	2.44	0.19	0.44	1.41	0	76	0
0.95	28.68	42.75	18.51	0.02	0.04	1.57	0	8	0
1.05	10.83	14.64	6.69	0.05	0.11	1.72	0	0	44
1.15	11.05	14.93	6.83	0.04	0.10	1.85	0	0	44
1.25	9.53	12.91	5.90	0.05	0.12	1.96	0	0	53
1.35	9.65	13.07	5.97	0.05	0.11	2.06	0	0	53
1.45	8.49	11.53	5.26	0.05	0.12	2.14	0	0	62
1.55	8.55	11.61	5.30	0.05	0.12	2.21	0	0	62
1.65	9.23	12.54	5.72	0.04	0.10	2.27	0	0	57
1.75	9.26	12.59	5.75	0.04	0.10	2.31	0	0	57
1.85	10.04	13.66	6.24	0.04	0.09	2.35	0	0	52
1.95	10.06	13.69	6.25	0.04	0.09	2.38	0	0	52
2.05	10.97	14.95	6.82	0.03	0.08	2.40	0	0	47
2.15	10.96	14.97	6.82	0.03	0.08	2.42	0	0	47

TABLE IV. Basic numbers for HETDEX, covering 420 sq. deg..

z	$\frac{\sigma_{DA/s}}{DA/s}$	$\frac{\sigma_{Hs}}{Hs}$	$\frac{\sigma_{R/s}}{R/s}$	$\bar{n}P_{0.2,0}$	$\bar{n}P_{0.14,0.6}$	V	$\frac{dN}{dz d\text{deg}^2}$
	%	%	%			$(h^{-1}\text{Gpc})^3$	
1.95	5.51	7.93	3.49	0.48	1.21	0.17	1190
2.05	5.50	7.90	3.48	0.48	1.19	0.17	1190
2.15	5.49	7.88	3.47	0.48	1.18	0.17	1190
2.25	5.47	7.86	3.46	0.47	1.16	0.17	1190
2.35	5.46	7.84	3.46	0.47	1.15	0.17	1190
2.45	5.45	7.82	3.45	0.47	1.14	0.17	1190
2.55	5.44	7.81	3.45	0.47	1.14	0.17	1190
2.65	5.44	7.81	3.44	0.47	1.13	0.17	1190
2.75	5.43	7.80	3.44	0.48	1.13	0.17	1190
2.85	5.42	7.80	3.43	0.48	1.13	0.17	1190
2.95	5.41	7.79	3.43	0.48	1.13	0.17	1190
3.05	5.40	7.79	3.43	0.48	1.13	0.17	1190
3.15	5.40	7.79	3.43	0.49	1.13	0.17	1190
3.25	5.39	7.79	3.43	0.49	1.14	0.16	1190
3.35	5.39	7.80	3.42	0.49	1.14	0.16	1190
3.45	5.38	7.80	3.42	0.50	1.14	0.16	1190

TABLE V. Basic numbers for DESI, covering 14000 sq. deg..

z	$\frac{\sigma_{DA/s}}{DA/s}$	$\frac{\sigma_{Hs}}{Hs}$	$\frac{\sigma_{R/s}}{R/s}$	$\bar{n}P_{0.2,0}$	$\bar{n}P_{0.14,0.6}$	V ($h^{-1}\text{Gpc}$) ³	$\frac{dN_{ELG}}{dz \text{ ddeg}^2}$	$\frac{dN_{LRG}}{dz \text{ ddeg}^2}$	$\frac{dN_{QSO}}{dz \text{ ddeg}^2}$	$\frac{\sigma_{f\sigma_{0.1}}}{f\sigma_{0.1}}$	$\frac{\sigma_{f\sigma_{0.2}}}{f\sigma_{0.2}}$
	%	%	%					%	%		
0.15	2.78	5.34	1.95	5.24	13.79	0.23	376	50	8	7.51	3.60
0.25	1.87	3.51	1.30	3.24	8.19	0.56	347	125	23	5.24	2.55
0.35	1.45	2.69	1.00	2.58	6.35	0.99	291	222	31	4.44	2.17
0.45	1.19	2.20	0.82	2.36	5.74	1.46	285	332	31	3.92	1.91
0.55	1.01	1.85	0.70	2.42	5.90	1.94	431	448	32	3.31	1.60
0.65	0.87	1.60	0.60	2.58	6.34	2.42	722	563	34	2.80	1.34
0.75	0.77	1.41	0.53	2.77	6.85	2.87	1112	675	37	2.47	1.18
0.85	0.76	1.35	0.52	2.05	5.17	3.29	1333	471	44	2.34	1.11
0.95	0.88	1.42	0.58	1.03	2.76	3.67	1401	91	50	2.34	1.13
1.05	0.91	1.41	0.59	0.82	2.24	4.01	1469	11	56	2.32	1.12
1.15	0.91	1.38	0.58	0.75	2.05	4.31	1483	0	62	2.30	1.12
1.25	0.91	1.36	0.58	0.69	1.86	4.57	1421	0	69	2.32	1.14
1.35	1.00	1.46	0.64	0.53	1.42	4.80	1120	0	75	2.45	1.26
1.45	1.17	1.66	0.74	0.38	1.00	4.99	775	0	81	2.71	1.47
1.55	1.50	2.04	0.93	0.25	0.63	5.15	460	0	83	3.22	1.89
1.65	2.36	3.15	1.45	0.13	0.33	5.29	179	0	80	4.63	3.06
1.75	3.62	4.87	2.23	0.08	0.19	5.40	49	0	77	7.17	5.14
1.85	4.79	6.55	2.98	0.06	0.13	5.49	0	0	74	10.26	7.66

use $b_{\text{ELG}}(z)D(z) = 0.84$ [103]. Finally, we use quasars as tracers of cosmic structure. Quasars are difficult to target photometrically, especially in the redshift range $2 < z < 3.5$, but can be very efficiently targeted using variability. They are very highly biased, but are limited by their limited number density, which is considerably lower than that of LRGs and ELGs. For quasars we use $b_{\text{QSO}}(z)D(z) = 1.2$, loosely based on [104].

Numbers we use for Fisher matrix projections are given in Table V.

The quasar luminosity function use for the Ly α forest calculation follows [105], for magnitude $g < 23$, with a 0.8 reduction in numbers to allow for targeting inefficiency. The spectral signal-to-noise ratio that we use, computed using the *BBspecsim* code [101], is shown in Figure 1. Note that we always absorb BOSS and eBOSS into DESI, as they will be physically overlapping (it was not necessary to combine BOSS and eBOSS because they cover distinct redshift ranges).

At the heart of the Ly α forest data at $z \sim 2.5$, $\bar{n}P(k = 0.14 \text{ hMpc}^{-1}, \mu = 0.6) = 0.09$ for DESI quasar clustering, while scaling from the Ly α forest BAO errors gives ~ 0.22 for the Ly α forest i.e., any corrections to the high-noise limit when combining the two will be modest, although we are on the borderline of applicability for this approximation. Note that we have not included reconstruction of the non-linear damping of the BAO feature, which might produce a small ($\sim 10 - 15\%$) improvement.

H. Euclid

We only include the redshift survey from Euclid, assuming 15000 sq. deg. and a total of 50 million galaxies, based on [106] (note that there is some uncertainty in the expected number of galaxies). Adding Euclid lensing should be qualitatively similar to LSST. Numbers we use for Euclid Fisher matrix projections are given in Table VI. We assume fiducial $b(z)D(z) = 0.76$. For simplicity, we assume Euclid does not overlap with DESI. To the extent that there is some overlap, there will be some degradation of combined constraints relative to what we quote (we do not see any case where this should critically change one's basic picture of how well parameters can be measured).

Note that the WFIRST-AFTA report [107] appears to suggest that these Euclid numbers are very optimistic. They forecast that Euclid will find factors of 8, 16, and 30 lower number density, at $z = 1.1, 1.5,$ and 1.9 , respectively, than they forecast for WFIRST, which correspond to factors 0.38, 0.49, and 0.49 smaller number density than we use in this paper – this would obviously lead to some degradation of our projections for Euclid.

I. WFIRST

We implement WFIRST-2.4 following [107]. Number densities come from their Table 2.2. The bias formula that we use for Euclid, $b(z)D(z) = 0.76$, happens to be exactly equal to the formula of [107], $b = 1.5 + 0.4(z - 1.5)$, at

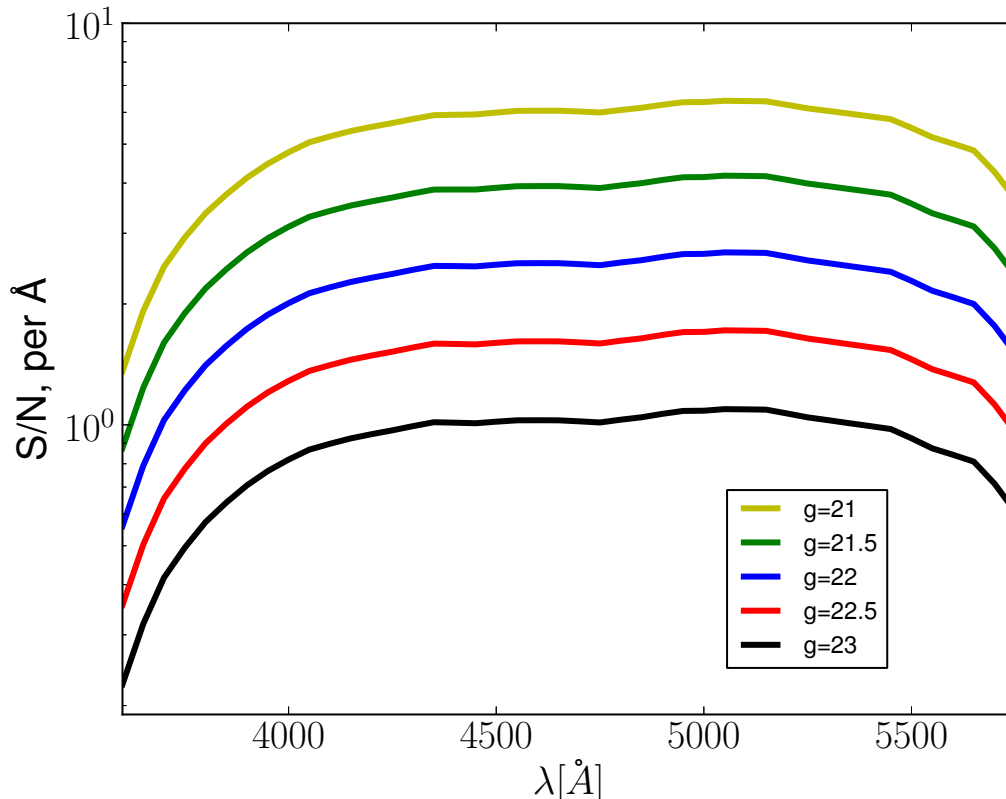


FIG. 1. Signal-to-noise ratio per \AA used for DESI quasar spectra (detector noise, not absorption noise), for different g magnitudes, accounting for mean $\text{Ly}\alpha$ forest absorption. (We only use the blue DESI spectrograph – we could squeeze out a little more BAO information at $z \gtrsim 3.7$ by including the red spectrograph.)

$z = 1.5$, and within 10% over the full redshift range, so we use this also for WFIRST. The numbers we use for Fisher projections are given in Table VII.

In the interest of limiting the length of our main results tables, we only include a limited set of cases using WFIRST.

J. Summary of S/N and BAO distance errors vs. redshift for redshift surveys

Coincidentally, the BAO scale and non-linear scale are quite similar, so BAO errors can summarize well the general relative constraining power of redshift surveys and their redshift dependence. The signal-to-noise for typical BAO-scale modes in redshift space is shown in Fig. 2. We evaluate $\bar{n}P$ at $k = 0.14 \text{ hMpc}^{-1}$, $\mu = 0.6$, an approximate center-of-weight point for BAO measurements. We chose the numbers 0.14 and 0.6 by looking for the point where $\bar{n}P = 1$ corresponded to the optimum in a trade-off between area and number density at fixed total number of objects (specifically, for the full range of parameters covered by DESI LRGs and ELGs). We think this definition reflects the origin of the idea that $\bar{n}P = 1$ is a special point, but it should be kept in mind that achieving $\bar{n}P$ by this definition does leave a survey significantly farther away from the sample variance limit than the traditional definition $k = 0.2 \text{ hMpc}^{-1}$, $\mu = 0$.

Projected BAO distance errors are shown in Fig. 3.

V. PHOTOMETRIC SURVEYS

We compute photometric survey Fisher matrices in terms of angular cross- and auto-power spectra, C_ℓ^{xy} , between objects divided up into nominal redshift bins based on photometric redshift estimates, i.e., photo- z 's (in case it is not obvious, the fundamental reason why it is natural to use different computational methods for redshift and photometric

TABLE VI. Basic numbers for Euclid (50 million total galaxies), covering 15000 sq. deg.. Note that the number densities here may be optimistic by a factor ~ 2 [107].

z	$\frac{\sigma_{DA/s}}{D_A/s}$ %	$\frac{\sigma_{Hs}}{Hs}$ %	$\frac{\sigma_{R/s}}{R/s}$ %	$\bar{n}P_{0.2,0}$	$\bar{n}P_{0.14,0.6}$	V $(h^{-1}\text{Gpc})^3$	$\frac{dN}{dz d\text{deg}^2}$
0.65	1.23	1.89	0.79	0.75	2.24	2.59	1100
0.75	0.83	1.42	0.56	1.69	5.03	3.07	2950
0.85	0.74	1.27	0.50	1.90	5.60	3.52	3800
0.95	0.71	1.19	0.48	1.75	5.11	3.93	3900
1.05	0.70	1.14	0.46	1.55	4.48	4.29	3775
1.15	0.70	1.12	0.46	1.35	3.85	4.62	3525
1.25	0.70	1.10	0.46	1.17	3.31	4.90	3250
1.35	0.73	1.11	0.47	0.98	2.74	5.14	2850
1.45	0.78	1.16	0.50	0.78	2.15	5.35	2350
1.55	0.87	1.24	0.55	0.59	1.62	5.52	1850
1.65	1.01	1.40	0.63	0.43	1.16	5.66	1375
1.75	1.23	1.64	0.75	0.30	0.80	5.78	975
1.85	1.61	2.07	0.97	0.20	0.52	5.88	650
1.95	2.32	2.90	1.38	0.12	0.31	5.95	400
2.05	5.32	6.39	3.11	0.04	0.12	6.01	150

TABLE VII. Basic numbers for WFIRST-2.4, covering 2000 sq. deg..

z	$\frac{\sigma_{DA/s}}{D_A/s}$ %	$\frac{\sigma_{Hs}}{Hs}$ %	$\frac{\sigma_{R/s}}{R/s}$ %	$\bar{n}P_{0.2,0}$	$\bar{n}P_{0.14,0.6}$	V $(h^{-1}\text{Gpc})^3$	$\frac{dN}{dz d\text{deg}^2}$
1.05	1.51	2.72	1.03	4.37	12.60	0.57	10623
1.15	1.43	2.56	0.98	4.50	12.85	0.62	11776
1.25	1.35	2.42	0.92	5.00	14.13	0.65	13877
1.35	1.29	2.30	0.88	5.33	14.90	0.69	15527
1.45	1.24	2.21	0.85	5.58	15.42	0.71	16890
1.55	1.23	2.16	0.84	5.04	13.79	0.74	15759
1.65	1.25	2.15	0.84	4.15	11.23	0.76	13305
1.75	1.28	2.16	0.86	3.33	8.94	0.77	10918
1.85	1.33	2.19	0.88	2.61	6.94	0.78	8697
1.95	1.41	2.27	0.93	1.99	5.25	0.79	6718
2.05	2.51	3.52	1.57	0.47	1.23	0.80	1610
2.15	2.60	3.62	1.62	0.44	1.14	0.81	1509
2.25	2.74	3.78	1.70	0.40	1.02	0.81	1368
2.35	3.02	4.09	1.86	0.33	0.85	0.81	1156
2.45	3.38	4.52	2.08	0.28	0.70	0.81	960
2.55	3.87	5.11	2.36	0.23	0.57	0.81	781
2.65	4.52	5.90	2.75	0.18	0.45	0.81	626
2.75	5.41	6.99	3.27	0.14	0.35	0.81	490

surveys is that redshift surveys derive most of their power from fluctuations on radial scales much smaller than the scale of cosmological evolution, while lensing surveys do not). Except when otherwise specified, we use all cross- and auto-correlations involving lensing and galaxy density in a set of tomographic bins of width $\Delta z = 0.2$ and maximum redshift $z_{\text{max}} = 2$, i.e., information from photometric galaxy clustering and galaxy-galaxy lensing are automatically included [108]. Bins in ℓ have size $\Delta \ln \ell = 0.2$. We assume no photo- z systematics, no intrinsic alignments, and no shear calibration bias. For shear-shear we use $\ell_{\text{max}} = 500$, to reflect the limitation set by non-linear effects [19, 109–111]. Overall our treatment of lensing is optimistic, at least relative to the FoMSWG treatment [19] (see Table XXV), but it is beyond the scope of this paper to get into lensing systematics in detail – these projections should be thought of as targets for lensing researchers to work towards.

In the rest of this section we give some more details describing our angular clustering treatment.

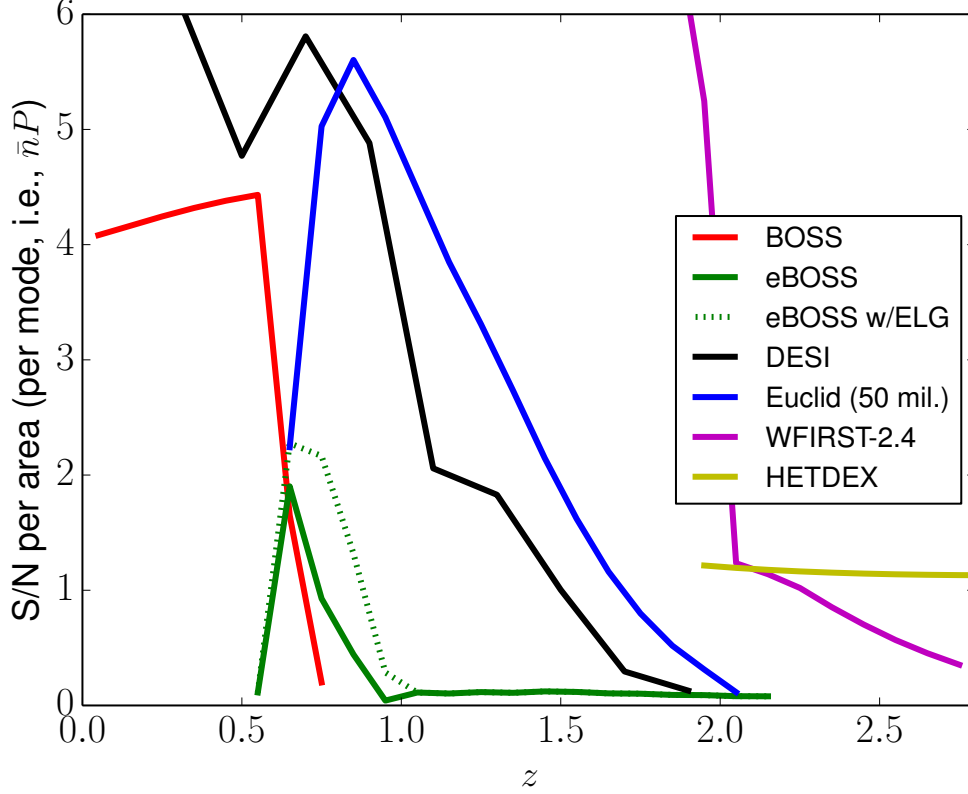


FIG. 2. $\bar{n}P(k = 0.14 \text{ hMpc}^{-1}, \mu = 0.6)$ comparison. DESI does not include the Ly α forest contribution, which would bring it to effective $\bar{n}P \sim 0.3$ at $z \sim 2.5$.

A. Angular Clustering

Suppose we define an angular field $\delta_{i,x}(\theta)$ as the redshift integral with weight $W_x(z)$ over a 3D field $\delta_i(z, \theta)$, i.e.,

$$\delta_{i,x}(\theta) = \int dz W_x(z) \delta_i(z, \theta) \quad (8)$$

(at this stage this is just a definition, but $\delta_i(z, \theta)$ could be the density of some type of galaxy, or mass density, with $W_x(z)$ the true redshift distribution of galaxies within some nominal photo- z bin, or lensing weight, for example). The angular correlation function of two such fields is

$$\xi_{ixjy}(\Delta\theta) = \int dz \int dz' W_x(z) W_y(z') \langle \delta_i(z, \theta) \delta_j(z', \theta + \Delta\theta) \rangle = \int d\bar{z} \int d\Delta z W_x(\bar{z}) W_y(\bar{z} + \Delta z) \xi_{ij}(\bar{z}, \Delta z, \Delta\theta) \quad (9)$$

where note that there is no approximation or loss of generality here, i.e., $\bar{z} = (z + z')/2$ and $\Delta z = z - z'$ are equally good parameters of two-point function evolving completely generally with redshift (although note that in general the sign of Δz does matter, i.e., we cannot use $|\Delta z|$). We can now FT $\xi_{ij}(\bar{z}, \Delta z, \Delta\theta)$ with respect to $\Delta\theta$ and Δz and plug that in to obtain

$$P_{xijy}(k_\theta) = \int d\bar{z} \int d\Delta z W_x(\bar{z}) W_y(\bar{z} + \Delta z) \int \frac{dk_z}{2\pi} \exp(-ik_z \Delta z) P_{ij}(\bar{z}, k_z, k_\theta) \quad (10)$$

Now we make an approximation, that the kernels $W(z)$ are broad enough that we can assume we are sensitive only to modes with small k_z , specifically k_z much less than k_θ , so that $P(k_z, k_\theta) \simeq P(0, k_\theta)$ (note that it would be fairly straightforward to include higher order terms in a Taylor expansion here). This allows us to integrate the exponential factor over k_z to obtain $2\pi\delta^D(\Delta z)$ and then

$$P_{xijy}(k_\theta) \simeq \int dz W_x(z) W_y(z) P_{ij}(z, k_z = 0, k_\theta) . \quad (11)$$

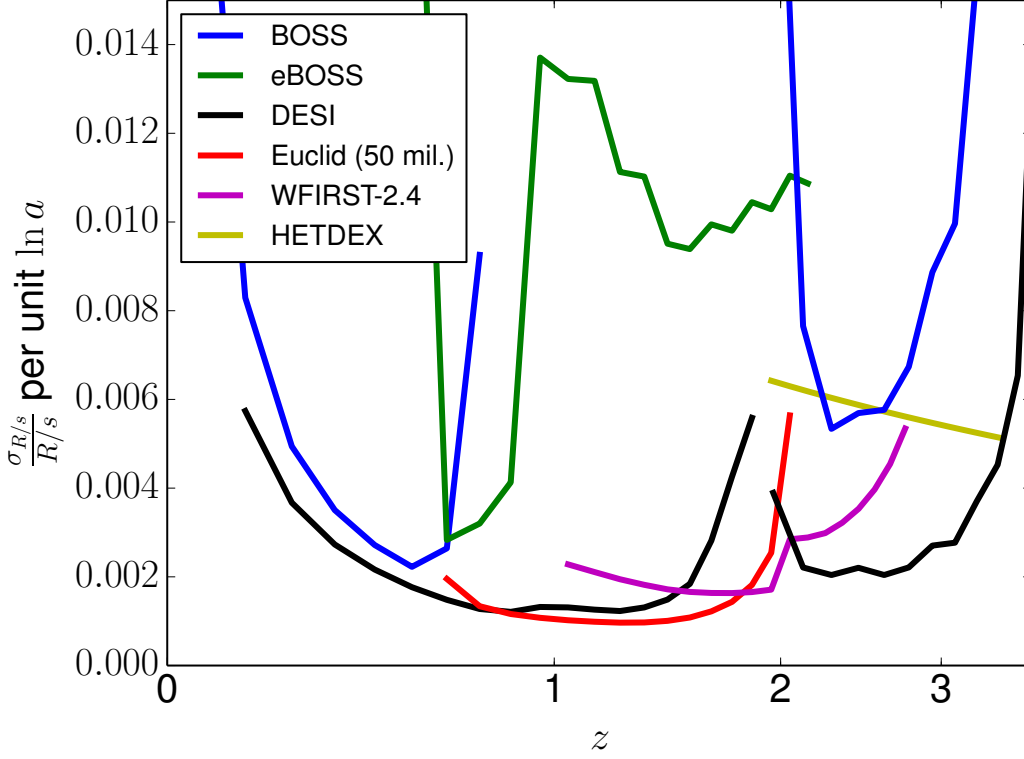


FIG. 3. Fractional error on the dilation factor as a function of redshift, per unit $\ln a$, i.e., in some sense a distance error *density* (plotting points aggregated over different bin widths, as is sometimes done, is essentially like plotting densities in different units on the same scale – of course, to add up information one still needs to integrate the inverse square of the curve). In other words, the effect of a width Δz is removed in this plot.

(Needless to say, this approximation breaks down as $k_\theta \rightarrow 0$, but there are few modes there so our calculation is not sensitive to this.) Note that the units of P_{ij} are redshift times angle squared, i.e., it is related to the usual comoving coordinate power spectrum, which we will identify by arguments k_\parallel and k_\perp , by

$$P_{ij}(z, k_z = 0, k_\theta) = \frac{H(z)/c}{r^2(z)} P_{ij}(z, k_\parallel = 0, k_\perp = k_\theta/r(z)) \quad (12)$$

The final step to obtain the usual Limber approximation equation is to identify k_θ with $\ell + 1/2$, and then $C_{xij}(\ell) = P_{xij}[k_\theta = \ell + 1/2]$, i.e.,

$$C_{xij}(\ell) = \int dz W_x(z) W_y(z) \frac{H(z)/c}{r^2(z)} P_{ij} \left(z, k_\parallel = 0, k_\perp = \frac{\ell + 1/2}{r(z)} \right). \quad (13)$$

This expression is often found in the literature (e.g., [112]), but this derivation may show more clearly the origin and units of the various factors.

B. Weight functions

1. Density

One simple example of the use of Eq. 13 is clustering of two types of galaxy, where $W(z) = n(z)/n_{tot}$ if $n(z) = dN/dz d\theta^2 = [r^2(z)c/H(z)]n_{com}(z)$ and $n_{tot} \equiv \int dz n(z)$, and in the usual linear regime picture $P_{ij}(z, 0, k_\perp) = b_i(z)b_j(z)P_m(k_\perp) + \delta_{ij}^K n_{com}^{-1}$ (n_{com} is the 3D comoving coordinate density). Weight functions here are defined in terms

of the *actual* redshift distribution of galaxies in a bin. For a bin defined by measured redshifts, the redshift errors must be accounted for.

Often we see the formula

$$n(z) \propto (z/z_*)^\alpha \exp\left[-(z/z_*)^\beta\right] \quad (14)$$

used for number densities. This can be integrated analytically to provide a normalization:

$$\int_0^\infty dz \left(\frac{z}{z_*}\right)^\alpha \exp\left[-\left(\frac{z}{z_*}\right)^\beta\right] = z_* \beta^{-1} \Gamma\left[\frac{\alpha+1}{\beta}\right] \quad (15)$$

E.g., for $\alpha = 2$, $\beta = 1$, the γ function evaluates to 2, so

$$\frac{dN}{dz}(z) = \frac{n_{tot}}{2z_*} \left(\frac{z}{z_*}\right)^2 \exp\left[-\frac{z}{z_*}\right] \quad (16)$$

2. Weak gravitational lensing

For weak lensing, the weight function is [113]:

$$W_\kappa(z_l) = \frac{3}{2} \Omega_{m,0} H_0^2 \frac{r(z_l)}{cH(z_l)a(z_l)} \int_{z_l}^\infty dz_s \frac{r(z_s) - r(z_l)}{r(z_s)} \frac{n(z_s)}{n_{tot}} \quad (17)$$

C. Non-linearity

We use the non-linear mass power spectrum for lensing-lensing correlations [114–116] and the linear power spectrum for everything else. To cut off the angular galaxy clustering before non-linear effects destroy its usefulness, we multiply the power spectrum of the galaxy field (including both clustering and noise) by $\exp\left[-(\ell/\ell_c)^2\right]$ when computing the error covariance matrix for $g-g$ and $g-\kappa$ correlations, where $\ell_c(z) = k_{\max,\text{eff}} r(z)$, $r(z)$ is the comoving angular diameter distance to redshift z , and $k_{\max,\text{eff}}$ is the maximum k used for the redshift survey. To be clear, this is a “soft” cutoff on ℓ , increasing the noise term (equivalent to suppressing the signal term, outside the Fisher derivative) as an alternative to simply truncating our calculation at some maximum ℓ . We introduced this Gaussian cutoff in an attempt to be slightly more realistic by allowing $g-\kappa$ to be sensitive to a somewhat smaller scale than $g-g$ (because it has only one power of the cutoff Gaussian instead of two), but it gives remarkably close to exactly the same result as a sharp cutoff.

D. Noise

Noise power is \bar{n}^{-1} for galaxy-galaxy auto-correlations, $\frac{0.3^2}{2}\bar{n}^{-1}$ for $\kappa-\kappa$ auto-correlations, where $0.3^2/2$ is from the intrinsic shape noise of galaxies [117].

E. C_ℓ covariance matrices

In our most standard angular calculation we divide the objects into $\Delta z = 0.2$ groupings by estimated redshift, spanning the range $0 < z < 2$. At the maximum, when we consider a lensing survey overlapping with a spectroscopic survey (in the Appendix), we have 4 tracers – LRGs, ELGs, photo-galaxy density, and photo-galaxy lensing – which gives 40 angular fields (for completeness we tried including lensing of LRGs and ELGs, but they made no contribution). From these we can measure 820 cross and auto correlations of the form $C_{\ell,ij}$. The covariance between two of these measurements is

$$\langle (C_{\ell,xy} - \langle C_{\ell,xy} \rangle) (C_{\ell,mn} - \langle C_{\ell,mn} \rangle) \rangle = (f_{\text{sky}} \Delta \ell (2\ell + 1))^{-1} (C_{\ell,xm} C_{\ell,yn} + C_{\ell,xn} C_{\ell,ym}) \quad (18)$$

where $\Delta \ell$ is the width of the bin in ℓ , f_{sky} is the fraction of the sky covered by the survey, and $C_{\ell s}$ include appropriate noise.

TABLE VIII. Abbreviations for experiments/sub-experiments in our tables.

Abbreviation	Data Set
<i>P</i>	Planck CMB (and a 5% constraint on H_0 that only matters in severely under-constrained cases).
<i>BgB</i>	BOSS galaxy BAO.
<i>BlB</i>	BOSS Ly α forest and high- z quasar BAO.
<i>BgAk</i> _{max,eff}	BOSS galaxy broadband to $k < k_{\text{max,eff}}$ $h\text{Mpc}^{-1}$ (plus BAO beyond that).
<i>DES</i>	DES lensing and galaxy clustering.
<i>hdB</i>	HETDEX BAO
<i>hdAk</i> _{max,eff}	HETDEX broadband to $k < k_{\text{max,eff}}$ $h\text{Mpc}^{-1}$ (plus BAO beyond that).
<i>ebgAk</i> _{max,eff}	eBOSS galaxy broadband to $k < k_{\text{max,eff}}$ $h\text{Mpc}^{-1}$ (plus BAO beyond that).
<i>BBgB</i>	DESI galaxy BAO.
<i>BBlB</i>	DESI Ly α forest and high- z quasar BAO.
<i>BBAk</i> _{max,eff}	DESI galaxy broadband to $k < k_{\text{max,eff}}$ $h\text{Mpc}^{-1}$ (plus BAO beyond that).
<i>euB</i>	Euclid BAO (for 50 million galaxies).
<i>euAk</i> _{max,eff}	Euclid galaxy broadband to $k < k_{\text{max,eff}}$ $h\text{Mpc}^{-1}$ (plus BAO beyond that).
<i>LSST</i>	LSST lensing and galaxy clustering.
<i>BlA</i>	BOSS Ly α forest broadband (including relatively small, $\sim 1\text{D}$ scales).
<i>l1D</i>	~ 100 high resolution Ly α forest spectra.
<i>BBlA</i>	DESI Ly α forest broadband (including relatively small, $\sim 1\text{D}$ scales).
<i>BB24</i>	24 is appended to BB to indicate 24000 sq. deg. DESI instead of the baseline 14000 sq. deg..
<i>wfB</i>	WFIRST BAO.
<i>wfAk</i> _{max,eff}	WFIRST galaxy broadband to $k < k_{\text{max,eff}}$ $h\text{Mpc}^{-1}$ (plus BAO beyond that).

F. Photo- z error distribution

For a given estimated photo- z , we assume a true distribution of galaxy redshifts following a simple Gaussian distribution with rms width $0.05(1+z)$. This propagates into the calculation through the weight kernels $W_x(z)$. In this paper we assume the distribution is exactly known, i.e., well-calibrated by direct redshift measurements.

G. DES

We include lensing, galaxy clustering, and their cross-correlations from DES, an imaging survey covering 5000 sq. deg. (www.darkenergysurvey.org). We use $\alpha = 1.25$, $\beta = 2.29$, $z_\star = 0.88$, and $n_{tot} = 12 \text{ arcmin}^{-2}$ in Eq. 14. For bias of DES galaxies we adopt using $b(z)D(z)/D(0) = 0.95$. This agrees well with halo number matching biases at $z \lesssim 1 - 1.5$, but is lower at higher z . We include a free bias parameter for each photo- z bin. In some circumstances this is optimistic, as generally galaxies with different true redshift within a photo- z bin can have different bias (this is important if, e.g., we want to calibrate photo- z errors by cross-correlation with a redshift survey [118–122]).

H. LSST

Similar to DES, for LSST [123], covering 20000 sq. deg., we use $\alpha = 2.0$, $\beta = 1.0$, $z_\star = 0.3$, and $n_{tot} = 50 \text{ arcmin}^{-2}$ in Eq. 14, with $b(z)D(z)/D(0) = 0.95$.

VI. PARAMETER CONSTRAINT PROJECTIONS

In this section we give parameter constraint projections for a large number of combinations of experiments and parameters.

A. Vanilla model (including neutrino mass!)

Table IX shows constraints in our baseline model, which may be of primary interest to readers interested in neutrino mass (see [124] for a review).

TABLE IX. Neutrino mass and other basic parameter projections. See Table VIII for experiment codes

	ω_m	ω_b	θ_s	Σm_ν	$\log_{10}(A)$	n_s	τ
value	0.141	0.0221	0.597	0.0600	-8.66	0.961	0.0920
P	0.0037	0.00015	0.00035	0.35	0.0039	0.0038	0.0045
$P + BgB + BlB$	0.00074	0.00015	0.00014	0.10	0.0038	0.0038	0.0044
$P + BgA0.1 + BlB$	0.00070	0.00013	0.00014	0.068	0.0037	0.0031	0.0044
$P + BgA0.2 + BlB$	0.00071	0.00012	0.00015	0.046	0.0037	0.0028	0.0043
$P + DES$	0.0013	0.00013	0.00017	0.041	0.0036	0.0032	0.0043
$P + BgB + BlB + DES$	0.00069	0.00011	0.00014	0.030	0.0035	0.0027	0.0043
$P + BgA0.1 + BlB + DES$	0.00067	0.00011	0.00014	0.029	0.0035	0.0027	0.0042
$P + BgA0.1 + BlB + ebA0.1$	0.00064	0.00012	0.00014	0.052	0.0037	0.0029	0.0043
$P + BgA0.2 + BlB + ebA0.2$	0.00064	0.00011	0.00014	0.036	0.0037	0.0027	0.0043
$P + BgA0.1 + BlB + ebA0.1 + DES$	0.00062	0.00011	0.00014	0.028	0.0035	0.0026	0.0042
$P + hdB + BgB$	0.00074	0.00015	0.00014	0.099	0.0038	0.0038	0.0044
$P + hdA0.1 + BgA0.1$	0.00069	0.00012	0.00014	0.061	0.0037	0.0030	0.0044
$P + hdA0.2 + BgA0.2$	0.00068	0.00011	0.00014	0.039	0.0037	0.0027	0.0043
$P + BBgB$	0.00055	0.00015	0.00014	0.090	0.0038	0.0038	0.0044
$P + BBgB + BlB$	0.00055	0.00015	0.00014	0.090	0.0038	0.0038	0.0044
$P + BBIB + BgB$	0.00072	0.00015	0.00014	0.098	0.0038	0.0038	0.0044
$P + BBgB + BBIB$	0.00055	0.00015	0.00014	0.090	0.0038	0.0038	0.0044
$P + BBgB + BBIB + DES$	0.00045	0.00011	0.00014	0.027	0.0035	0.0025	0.0043
$P + BBgA0.1$	0.00044	0.00011	0.00014	0.024	0.0036	0.0024	0.0043
$P + BBgA0.1 + BBIB$	0.00044	0.00011	0.00014	0.024	0.0036	0.0024	0.0043
$P + BBgA0.1 + BBIB + DES$	0.00043	0.00011	0.00014	0.021	0.0034	0.0024	0.0041
$P + BBgA0.2 + BBIB$	0.00042	0.00010	0.00014	0.017	0.0035	0.0022	0.0043
$P + BBgA0.2 + BBIB + DES$	0.00042	0.00010	0.00014	0.017	0.0033	0.0022	0.0040
$P + BB2gB + BB2IB$	0.00052	0.00015	0.00014	0.088	0.0038	0.0037	0.0044
$P + BB2gA0.1 + BB2IB$	0.00039	0.00011	0.00014	0.020	0.0035	0.0023	0.0043
$P + BB2gA0.1 + BB2IB + DES$	0.00038	0.00011	0.00013	0.019	0.0033	0.0023	0.0040
$P + BB2gA0.2 + BB2IB$	0.00037	9.9e-05	0.00014	0.015	0.0035	0.0020	0.0042
$P + BB2gA0.2 + BB2IB + DES$	0.00037	9.9e-05	0.00013	0.015	0.0032	0.0020	0.0040
$P + BgB + BlB + euB$	0.00054	0.00015	0.00014	0.090	0.0038	0.0038	0.0044
$P + BgA0.1 + BlB + euA0.1$	0.00043	0.00011	0.00014	0.021	0.0036	0.0024	0.0043
$P + BgA0.1 + BlB + euA0.1 + DES$	0.00043	0.00011	0.00014	0.019	0.0034	0.0023	0.0041
$P + BgA0.2 + BlB + euA0.2$	0.00042	0.00010	0.00014	0.015	0.0035	0.0021	0.0042
$P + BgA0.2 + BlB + euA0.2 + DES$	0.00041	0.00010	0.00014	0.015	0.0033	0.0021	0.0040
$P + BB2gA0.1 + BB2IB + euA0.1$	0.00036	0.00010	0.00013	0.017	0.0035	0.0022	0.0042
$P + BB2gA0.1 + BB2IB + euA0.1 + DES$	0.00036	0.00010	0.00013	0.016	0.0032	0.0022	0.0040
$P + BB2gA0.2 + BB2IB + euA0.2$	0.00034	9.6e-05	0.00013	0.014	0.0034	0.0018	0.0041
$P + BB2gA0.2 + BB2IB + euA0.2 + DES$	0.00034	9.6e-05	0.00013	0.013	0.0032	0.0018	0.0039
$P + LSST$	0.00080	0.00011	0.00015	0.020	0.0030	0.0029	0.0036
$P + BgB + BlB + LSST$	0.00060	0.00011	0.00014	0.018	0.0030	0.0025	0.0036
$P + BBgB + BBIB + LSST$	0.00044	0.00011	0.00013	0.016	0.0030	0.0022	0.0036
$P + BBgA0.1 + BBIB + LSST$	0.00042	0.00010	0.00013	0.015	0.0028	0.0021	0.0034
$P + BBgA0.2 + BBIB + LSST$	0.00041	0.00010	0.00013	0.014	0.0026	0.0020	0.0032
$P + BB2gA0.1 + BB2IB + LSST$	0.00038	0.00010	0.00013	0.015	0.0027	0.0020	0.0033
$P + BB2gA0.2 + BB2IB + LSST$	0.00036	9.8e-05	0.00013	0.013	0.0025	0.0018	0.0031
$P + BB2gA0.1 + BB2IB + euA0.1 + LSST$	0.00035	0.00010	0.00013	0.014	0.0026	0.0019	0.0032
$P + BB2gA0.2 + BB2IB + euA0.2 + LSST$	0.00033	9.5e-05	0.00013	0.011	0.0024	0.0016	0.0030
$P + wfB + BgB$	0.00064	0.00015	0.00014	0.095	0.0038	0.0038	0.0044
$P + wfA0.1 + BgA0.1$	0.00058	0.00011	0.00014	0.037	0.0037	0.0027	0.0043
$P + wfA0.2 + BgA0.2$	0.00056	0.00011	0.00014	0.021	0.0036	0.0025	0.0043
$P + BgB + BlA + l1D$	0.00066	0.00011	0.00014	0.053	0.0037	0.0032	0.0044
$P + BgA0.1 + BlA + l1D$	0.00065	0.00011	0.00014	0.048	0.0037	0.0030	0.0043
$P + BgA0.2 + BlA + l1D$	0.00066	0.00011	0.00014	0.040	0.0037	0.0027	0.0043
$P + BBgB + BBIA + l1D$	0.00041	0.00010	0.00014	0.039	0.0037	0.0029	0.0043
$P + BBgA0.1 + BBIA + l1D$	0.00039	0.00010	0.00014	0.023	0.0035	0.0021	0.0043
$P + BBgA0.2 + BBIA + l1D$	0.00038	0.00010	0.00014	0.017	0.0035	0.0019	0.0042
$P + BB2gB + BB2IA + l1D$	0.00036	0.00010	0.00014	0.034	0.0036	0.0028	0.0043
$P + BB2gA0.1 + BB2IA + l1D$	0.00035	0.00010	0.00013	0.019	0.0035	0.0019	0.0042
$P + BB2gA0.2 + BB2IA + l1D$	0.00034	9.8e-05	0.00014	0.015	0.0034	0.0016	0.0041
$P + BB2gA0.2 + BB2IA + l1D + euA0.2$	0.00032	9.5e-05	0.00013	0.013	0.0033	0.0015	0.0040
$P + BB2gA0.2 + BB2IA + l1D + LSST$	0.00033	9.7e-05	0.00013	0.012	0.0025	0.0015	0.0031
$P + BB2gA0.2 + BB2IA + l1D + euA0.2 + LSST$	0.00032	9.5e-05	0.00013	0.011	0.0024	0.0014	0.0030

We see that the 14000 sq. deg. baseline DESI can measure neutrino masses to 0.024 eV for $k_{\text{max,eff}} = 0.1 \text{ hMpc}^{-1}$ or 0.017 eV for $k_{\text{max,eff}} = 0.2 \text{ hMpc}^{-1}$. DES can improve the more pessimistic number to 0.021 eV, i.e., by the end of the DESI baseline survey the minimal neutrino mass of 0.057 eV should definitely be detected at $\sim 3\sigma$. Euclid's redshift survey can produce similar measurements. (Note that Euclid lensing can presumably be substituted for LSST here without a qualitative change in results.)

[125] found qualitatively similar expectations for Euclid, as did [126]. [127] appear to have found somewhat weaker constraints for the Euclid redshift survey, but it is not clear that they fully include the measurement that comes from redshift space distortions. [128, 129] found 0.01 – 0.02 eV constraints from Euclid using only the photometric survey, i.e., not including the redshift survey, but including clusters (amounting to a largely independent form of measurement from our redshift survey projections). [130] found qualitatively similar, although not very directly comparable, results for a futuristic 21 cm equivalent of a redshift survey. They found CMB lensing in the form of CMBpol to be somewhat more limited than our galaxy lensing experiments, producing an error $\sim 0.05\text{eV}$. We find [131] to be a little confusing to read, but a bottom line appears to be that their proposed CORE CMB lensing experiment could measure Σm_ν to ~ 0.02 eV when combined with BAO measurements (from CMB lensing alone they appear to be consistent with [130]). [132] found some combinations of future experiments reaching the 0.02-0.03 eV level, but do not appear to have included a full redshift survey. The LSST project book [123] quotes an error 0.03 – 0.07 eV depending on their fiducial Σm_ν value, not as good as our 0.02 eV projections for them, but they appear to be using only lensing-lensing correlations for this calculation, not including correlations involving galaxy density. Generally, the idea that ~ 0.02 eV level constraints will be achieved by cosmological measurements in the 2020's appears very secure – it is projected redundantly for several different kinds of probes, which are unlikely to all fail. A constraint ~ 0.01 eV is definitely possible.

1. Neutrino mass hierarchy

There is great interest in determining the distribution of masses between neutrino species [133]. Although cosmology can, in principle, measure individual neutrino mass eigenstates, this is unrealistic at the level of precision of experiments discussed here [134–138] and therefore we are effectively limited to determining only the sum of neutrino masses directly. The situation given experimental constraints is illustrated in Figure 4. In the case where the hierarchy is in fact normal with sum of masses near the minimum, i.e., sum of masses ~ 57 meV, the fact that the hierarchy is normal can be proven, because the minimum total mass in the inverted hierarchy is ~ 96 meV, however, if the hierarchy is inverted, or normal but with mass much above the minimum, there will be no possibility of distinguishing the two cases. We see that in the best case the experiments in Table IX can hope to distinguish the hierarchy at about 3.5σ level.

B. Dark Energy Figures of Merit

Table XI shows Dark Energy Task Force (DETF) Figures of Merit (FoMs) [140], except with the DETF definition modified to include marginalization over neutrino mass. For the common normalization convention that we follow, the FoM is simply $(\sigma_{w_p} \sigma_{w'})^{-1}$ where $w(z) = w_p + (a_p - a)w'$ and a_p is chosen to make the errors on w_p and w' independent.

We see that when neutrino mass uncertainty is accounted for it becomes more critical to include a probe sensitive to the amplitude/growth of structure, either broadband galaxy power or lensing or ideally both. This does not mean BAO is not very valuable – e.g., lensing alone does not do well either, while being greatly enhanced by isolated BAO, and of course all of our galaxy broadband constraints fully include BAO – there is just an extra degeneracy between dark energy and neutrino mass that can be decisively broken by a probe sensitive to perturbation amplitude. This is easy to understand qualitatively: the neutrinos act as essentially a form of modified gravity, breaking what we usually think of as the GR relation between background evolution and growth of structure. Overall we find the complementarity between different experiments striking – each of the major experiments contributes significantly and non-redundantly to building up our understanding of dark energy properties. Table XIII shows broader constraints in the FoM parameter space.

C. Modified Gravity

Table XV shows constraints on the FoMSWG [19] modified gravity parameters (as we interpret them above).

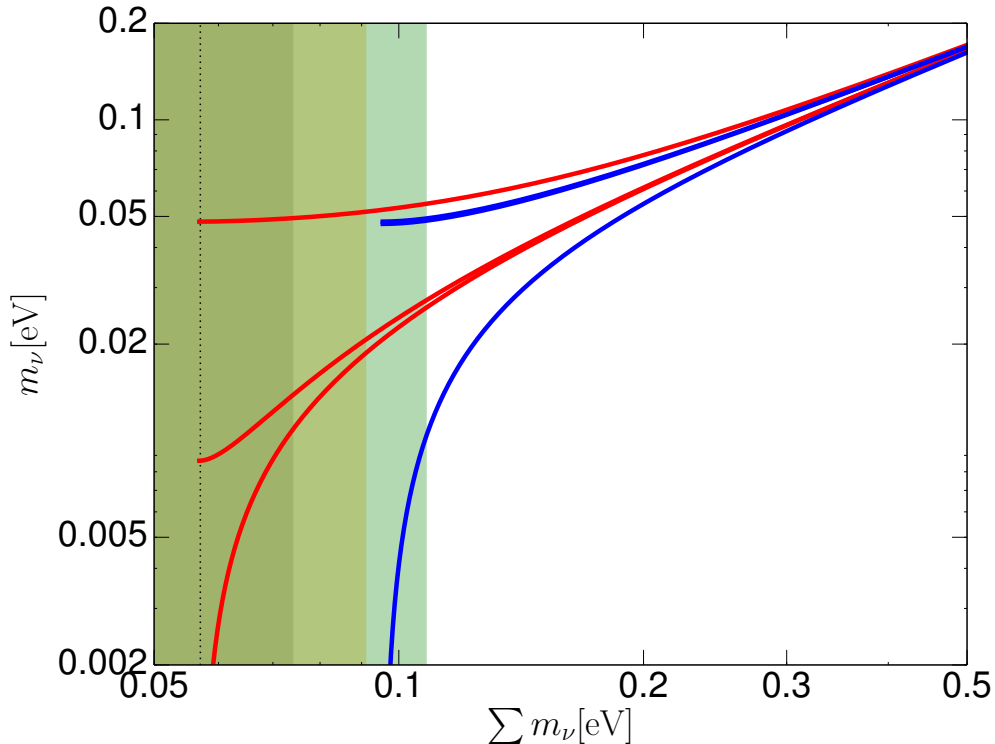


FIG. 4. Inverted (blue) vs. normal (red) hierarchies, given the current mass-squared difference measurements from [139]. Each line shows the mass of one of the neutrinos, plotted as a function of the sum of masses in each case (in the inverted case the two most massive neutrinos have almost indistinguishable mass on this plot). The green bands indicate the 1,2 and 3 sigma error in the reach of an experiment assuming no prior on $\sum m_\nu$ for a fiducial model with $\sum m_\nu = 0.057\text{eV}$ and $\sigma_{m_\nu} = 0.017\text{eV}$.

One thing we note is that neutrino masses are substantially degraded by including the MoG parameters, indicating that the $\sum m_\nu$ constraint is driven measuring the low- z structure amplitude relative to the CMB, more than the scale dependence of the neutrino power suppression, which would not be degenerate with these MoG parameters.

D. Inflation

We consider two ways to probe inflation: measurement of the scale dependence of the initial perturbations, and their level of Gaussianity.

1. Running of the spectral index

Table XVII shows constraints with free running of the spectral index.

We first note that previous tables, like this one, have shown that galaxy surveys can improve the constraint on n_s by about a factor of 2 relative to Planck alone (similar constraints have been projected for CMBpol [27]). We see that the Ly α forest broadband constraint is important for achieving the tightest constraints on α_s , i.e., starting from a Planck-only baseline of 0.0054, aggressive galaxy clustering from DESI and Euclid, combined with LSST, can reach an error 0.0028, while 0.0016 can be achieved with the Ly α forest broadband power, a critical improvement in the quest to find expected deviations from a pure power law at the 10^{-3} level. The statistical power of the DESI Ly α forest data will also help to control systematics and extensions of the gas model, and might allow further improvements if external data sets that are limiting the measurement are improved.

2. Non-Gaussianity (f_{NL})

In this section we do not attempt to be as comprehensive as others. We simply give the estimated constraining power for the main redshift surveys, based on the power spectrum, for the local model of non-Gaussianity, following [58, 141]. Table XIX shows the projections. The results are weakly sensitive to redshift binning (which sets the interval of free bias parameters), e.g., the DESI number would be 3.4 instead of 3.8 for $\Delta z = 0.2$ instead of the usual 0.1. The DESI high- z quasars ($z > 1.9$) add what might be considered a surprising amount to the constraint – it would be 4.7 instead of 3.8 without them (we do not use the Ly α forest here because we suspect that things like radiation background fluctuations will make it difficult to use the very largest scales for this kind of measurement [82]).

The $\sigma_{f_{\text{NL}}} \sim 5$ constraints possible with DESI or Euclid are comparable to Planck constraints [142]. It may be possible to do better using the bispectrum [143–148].

E. Dark radiation (N_ν)

Table XXI shows constraints on extra radiation beyond the standard amount contributed by photons and neutrinos, parameterized as is traditional by an effective number of neutrino species N_ν [149–152]. DESI-era LSS measurements should be able to verify if recent hints for extra radiation are correct [153]. If they are, a new quest will begin to measure the properties of the radiation in detail – if not, we can continue to search at higher precision. A constraint $\sigma_{N_{\text{eff}}} \sim 0.044$ has been projected for CMB lensing from CMBPol [27, 28].

VII. DISCUSSION AND CONCLUSIONS

Our choice of experiments is undoubtedly a somewhat subjective combination of predictability of results, likelihood to happen, and simply author capabilities and interest. In the future we might hope to add CMB lensing [130, 131, 154], higher resolution CMB experiments [155], 21 cm intensity mapping surveys [156–160], etc.. Our choice of cosmological models to project was also limited largely by author capability. We could hope to add projections for, e.g., other models of non-Gaussianity [161–177], warm dark matter [178–180] or primordial black holes contributing to the power spectrum [181, 182] (for the latter two we would really like to have a better Ly α forest implementation). In general there is more information in all of the data sets than we include here, e.g., obtainable by measuring higher order statistics like the bispectrum [183]. There is also a lot of work to be done to systematically quantify sensitivity to various potential systematic errors [184].

This is intended primarily as a reference paper, i.e., when you wonder how well we hope to measure parameters in a given scenario, you can look it up in the appropriate table. However, some of the initial take-home points, not all new to this paper but in any case quantified and highlighted, might be:

- Redshift surveys like DESI, with help from Planck and possibly lensing surveys, will measure the sum of neutrino masses to $\sim 0.01 - 0.02$ eV in the 2020's.
- Because they will inevitably be relevant, we should always include neutrino mass uncertainty in projections for other parameters. This introduces significant new uncertainty in dark energy measurements using exclusively BAO information from redshift surveys – the surveys will be much more powerful if we can accurately measure and model the broadband power spectrum.
- Using the Ly α forest enhanced by cross-correlation with quasar density, DESI will be able to make very precise BAO measurements at $z > 2$, one of its unique advantages over a survey like Euclid.
- Redshift surveys and lensing surveys are highly complementary as dark energy probes. (Somewhat surprisingly, however, overlapping the volume of the two such surveys does not bring significant new information as discussed in the Appendix, VIII B.)
- Allowing for deviations from GR significantly degrades neutrino mass constraints, highlighting the fact that these constraints at their most powerful come from measuring the amplitude of fluctuations at low redshift relative to the CMB (with redshift-space distortions for spectroscopic surveys or lensing for photometric surveys), more than measuring the effect of neutrinos on the shape of the power spectrum.
- Ly α forest power spectrum measurements are potentially our best probe of the running of the inflationary spectral index, while galaxy clustering can help to improve constraints on non-Gaussianity and the spectral index itself, relative to Planck.

We thank Yan-Chuan Cai for invaluable spot-checks of the lensing/redshift survey overlap calculations, and Zhaoming Ma for helpful conversations and the DES numbers.

-
- [1] A. Albrecht, G. Bernstein, R. Cahn, W. L. Freedman, J. Hewitt, *et al.*, ArXiv e-prints (2006), arXiv:astro-ph/0609591 [astro-ph].
- [2] B. A. Bassett, Y. Fantaye, R. Hlozek, and J. Kotze, *Int.J.Mod.Phys.* **D20**, 2559 (2011), arXiv:0906.0993 [astro-ph.CO].
- [3] A. R. Cooray, *Astron.Astrophys.* **348**, 31 (1999), arXiv:astro-ph/9904246 [astro-ph].
- [4] T. Giannantonio, C. Porciani, J. Carron, A. Amara, and A. Pillepich, *Mon.Not.Roy.Astron.Soc.* **422**, 2854 (2012), arXiv:1109.0958 [astro-ph.CO].
- [5] D. Huterer, M. Takada, G. Bernstein, and B. Jain, *Mon.Not.Roy.Astron.Soc.* **366**, 101 (2006), arXiv:astro-ph/0506030 [astro-ph].
- [6] J. Hamann, S. Hannestad, and Y. Y. Wong, *JCAP* **1211**, 052 (2012), arXiv:1209.1043 [astro-ph.CO].
- [7] S. Joudaki and M. Kaplinghat, *Phys.Rev.* **D86**, 023526 (2012), arXiv:1106.0299 [astro-ph.CO].
- [8] T. D. Kitching and A. Amara, *Mon. Not. Roy. Astron. Soc.* **398**, 2134 (2009), arXiv:0905.3383 [astro-ph.CO].
- [9] S. More, F. van den Bosch, M. Cacciato, A. More, H. Mo, *et al.*, *Mon.Not.Roy.Astron.Soc.* **430**, 747 (2013), arXiv:1207.0004 [astro-ph.CO].
- [10] D. H. Weinberg, M. J. Mortonson, D. J. Eisenstein, C. Hirata, A. G. Riess, and E. Rozo, ArXiv e-prints (2012), arXiv:1201.2434 [astro-ph.CO].
- [11] L. Wolz, M. Kilbinger, J. Weller, and T. Giannantonio, *JCAP* **1209**, 009 (2012), arXiv:1205.3984 [astro-ph.CO].
- [12] S. Khedekar and S. Majumdar, *JCAP* **1302**, 030 (2013), arXiv:1210.5586 [astro-ph.CO].
- [13] T. Basse, O. E. Bjaelde, J. Hamann, S. Hannestad, and Y. Y. Y. Wong, ArXiv e-prints (2013), arXiv:1304.2321 [astro-ph.CO].
- [14] M. C. A. Cerbolini, B. Sartoris, J.-Q. Xia, A. Biviano, S. Borgani, *et al.*, ArXiv e-prints (2013), arXiv:1303.4550 [astro-ph.CO].
- [15] A. R. Pullen and C. M. Hirata, ArXiv e-prints (2012), arXiv:1212.4500 [astro-ph.CO].
- [16] A. J. Ross *et al.* (BOSS Collaboration), *Mon.Not.Roy.Astron.Soc.* **424**, 564 (2012), arXiv:1203.6499 [astro-ph.CO].
- [17] W. Hu, in *ASP Conf. Ser. 339: Observing Dark Energy* (2005) pp. 215–+.
- [18] Planck Collaboration, P. A. R. Ade, N. Aghanim, C. Armitage-Caplan, M. Arnaud, M. Ashdown, F. Atrio-Barandela, J. Aumont, C. Baccigalupi, A. J. Banday, and *et al.*, ArXiv e-prints (2013), arXiv:1303.5076 [astro-ph.CO].
- [19] A. Albrecht, L. Amendola, G. Bernstein, D. Clowe, D. Eisenstein, L. Guzzo, C. Hirata, D. Huterer, R. Kirshner, E. Kolb, and R. Nichol, ArXiv e-prints (2009), arXiv:0901.0721.
- [20] E. V. Linder, *Phys. Rev. D* **79**, 063519 (2009), arXiv:0901.0918 [astro-ph.CO].
- [21] U. Seljak and M. Zaldarriaga, *Astrophys. J.* **469**, 437 (1996).
- [22] A. Lewis, A. Challinor, and A. Lasenby, *Astrophys. J.* **538**, 473 (2000).
- [23] W. Hu, *Phys. Rev. D* **65**, 023003 (2002), arXiv:astro-ph/0108090.
- [24] The Planck Collaboration, ArXiv Astrophysics e-prints (2006), arXiv:astro-ph/0604069.
- [25] J. R. Bond, C. Contaldi, A. Lewis, and D. Pogosyan, *International Journal of Theoretical Physics* **43**, 599 (2004), arXiv:astro-ph/0406195.
- [26] C. Howlett, A. Lewis, A. Hall, and A. Challinor, *JCAP* **4**, 027 (2012), arXiv:1201.3654 [astro-ph.CO].
- [27] S. Galli, M. Martinelli, A. Melchiorri, L. Pagano, B. D. Sherwin, and D. N. Spergel, *Phys. Rev. D* **82**, 123504 (2010), arXiv:1005.3808 [astro-ph.CO].
- [28] A. Melchiorri, S. Galli, M. Martinelli, and L. Pagano, *Journal of Physics Conference Series* **259**, 012004 (2010).
- [29] P. McDonald and A. Roy, *JCAP* **8**, 020 (2009), arXiv:0902.0991 [astro-ph.CO].
- [30] T. Baldauf, U. Seljak, V. Desjacques, and P. McDonald, *Phys. Rev. D* **86**, 083540 (2012), arXiv:1201.4827 [astro-ph.CO].
- [31] P. McDonald, *Phys. Rev. D* **74**, 103512 (2006).
- [32] V. Desjacques, *Phys. Rev. D* **87**, 043505 (2013), arXiv:1211.4128 [astro-ph.CO].
- [33] N. Kaiser, *Mon. Not. Roy. Astron. Soc.* **227**, 1 (1987).
- [34] D. Jeong and E. Komatsu, *Astrophys. J.* **691**, 569 (2009), arXiv:0805.2632.
- [35] U. Seljak and P. McDonald, *JCAP* **11**, 039 (2011), arXiv:1109.1888 [astro-ph.CO].
- [36] A. J. Nishizawa, M. Takada, and T. Nishimichi, *Mon. Not. Roy. Astron. Soc.* **433**, 209 (2013), arXiv:1212.4025 [astro-ph.CO].
- [37] X. Wang and A. Szalay, *Phys. Rev. D* **86**, 043508 (2012), arXiv:1204.0019 [astro-ph.CO].
- [38] K. C. Chan, R. Scoccimarro, and R. K. Sheth, *Phys. Rev. D* **85**, 083509 (2012), arXiv:1201.3614 [astro-ph.CO].
- [39] T. Matsubara, *Phys. Rev. D* **83**, 083518 (2011), arXiv:1102.4619 [astro-ph.CO].
- [40] Y.-S. Song, T. Nishimichi, A. Taruya, and I. Kayo, *Phys. Rev. D* **87**, 123510 (2013), arXiv:1301.3133 [astro-ph.CO].
- [41] Z. Vlah, U. Seljak, P. McDonald, T. Okumura, and T. Baldauf, *JCAP* **11**, 009 (2012), arXiv:1207.0839 [astro-ph.CO].
- [42] T. Okumura, U. Seljak, and V. Desjacques, *JCAP* **11**, 014 (2012), arXiv:1206.4070 [astro-ph.CO].
- [43] J. R. Shaw and A. Lewis, *Phys. Rev. D* **78**, 103512 (2008), arXiv:0808.1724.
- [44] D. Baumann, A. Nicolis, L. Senatore, and M. Zaldarriaga, *JCAP* **7**, 051 (2012), arXiv:1004.2488 [astro-ph.CO].
- [45] H.-J. Seo, J. Eckel, D. J. Eisenstein, K. Mehta, M. Metchnik, N. Padmanabhan, P. Pinto, R. Takahashi, M. White, and

- X. Xu, *Astrophys. J.* **720**, 1650 (2010), arXiv:0910.5005 [astro-ph.CO].
- [46] H.-J. Seo and D. J. Eisenstein, *Astrophys. J.* **665**, 14 (2007), arXiv:astro-ph/0701079.
- [47] M. White, ArXiv e-prints (2010), arXiv:1004.0250 [astro-ph.CO].
- [48] B. D. Sherwin and M. Zaldarriaga, *Phys. Rev. D* **85**, 103523 (2012), arXiv:1202.3998 [astro-ph.CO].
- [49] W. Ngan, J. Harnois-Déraps, U.-L. Pen, P. McDonald, and I. MacDonald, *Mon. Not. Roy. Astron. Soc.* **419**, 2949 (2012), arXiv:1106.5548 [astro-ph.CO].
- [50] A. Taruya, T. Nishimichi, S. Saito, and T. Hiramatsu, *Phys. Rev. D* **80**, 123503 (2009), arXiv:0906.0507 [astro-ph.CO].
- [51] C. Alcock and B. Paczynski, *Nature (London)* **281**, 358 (1979).
- [52] T. Okumura, U. Seljak, P. McDonald, and V. Desjacques, *JCAP* **2**, 010 (2012), arXiv:1109.1609 [astro-ph.CO].
- [53] H. Gil-Marín, C. Wagner, L. Verde, C. Porciani, and R. Jimenez, *JCAP* **11**, 029 (2012), arXiv:1209.3771 [astro-ph.CO].
- [54] A. Taruya, T. Nishimichi, and F. Bernardeau, *Phys. Rev. D* **87**, 083509 (2013), arXiv:1301.3624 [astro-ph.CO].
- [55] A. Vallinotto and E. V. Linder, ArXiv e-prints (2013), arXiv:1307.2906 [astro-ph.CO].
- [56] E. V. Linder and J. Samsing, *JCAP* **2**, 025 (2013), arXiv:1211.2274 [astro-ph.CO].
- [57] M. Crocce and R. Scoccimarro, *Phys. Rev. D* **77**, 023533 (2008), arXiv:0704.2783.
- [58] P. McDonald and U. Seljak, *JCAP* **10**, 007 (2009), arXiv:0810.0323.
- [59] P. McDonald, U. Seljak, S. Burles, D. J. Schlegel, D. H. Weinberg, R. Cen, D. Shih, J. Schaye, D. P. Schneider, N. A. Bahcall, J. W. Briggs, J. Brinkmann, R. J. Brunner, M. Fukugita, J. E. Gunn, Ž. Ivezić, S. Kent, R. H. Lupton, and D. E. Vanden Berk, *ApJS* **163**, 80 (2006), arXiv:astro-ph/0405013.
- [60] A. Slosar, A. Font-Ribera, M. M. Pieri, J. Rich, J.-M. Le Goff, É. Aubourg, J. Brinkmann, N. Busca, B. Carithers, R. Charlassier, M. Cortés, R. Croft, K. S. Dawson, D. Eisenstein, J.-C. Hamilton, S. Ho, K.-G. Lee, R. Lupton, P. McDonald, B. Medolin, D. Muna, J. Miralda-Escudé, A. D. Myers, R. C. Nichol, N. Palanque-Delabrouille, I. Pâris, P. Petitjean, Y. Piškur, E. Rollinde, N. P. Ross, D. J. Schlegel, D. P. Schneider, E. Sheldon, B. A. Weaver, D. H. Weinberg, C. Yèche, and D. G. York, *JCAP* **9**, 1 (2011), arXiv:1104.5244 [astro-ph.CO].
- [61] P. McDonald and D. J. Eisenstein, *Phys. Rev. D* **76**, 063009 (2007), arXiv:astro-ph/0607122.
- [62] P. McDonald, *Astrophys. J.* **585**, 34 (2003), arXiv:astro-ph/0108064.
- [63] N. G. Busca, T. Delubac, J. Rich, S. Bailey, A. Font-Ribera, D. Kirkby, J.-M. Le Goff, M. M. Pieri, A. Slosar, É. Aubourg, J. E. Bautista, D. Bizyaev, M. Blomqvist, A. S. Bolton, J. Bovy, H. Brewington, A. Borde, J. Brinkmann, B. Carithers, R. A. C. Croft, K. S. Dawson, G. Ebelke, D. J. Eisenstein, J.-C. Hamilton, S. Ho, D. W. Hogg, K. Honscheid, K.-G. Lee, B. Lundgren, E. Malanushenko, V. Malanushenko, D. Margala, C. Maraston, K. Mehta, J. Miralda-Escudé, A. D. Myers, R. C. Nichol, P. Noterdaeme, M. D. Olmstead, D. Oravetz, N. Palanque-Delabrouille, K. Pan, I. Pâris, W. J. Percival, P. Petitjean, N. A. Roe, E. Rollinde, N. P. Ross, G. Rossi, D. J. Schlegel, D. P. Schneider, A. Sheldon, E. S. Sheldon, A. Simmons, S. Snedden, J. L. Tinker, M. Viel, B. A. Weaver, D. H. Weinberg, M. White, C. Yèche, and D. G. York, *Astron. Astrophys.* **552**, A96 (2013), arXiv:1211.2616 [astro-ph.CO].
- [64] A. Slosar, V. Iršič, D. Kirkby, S. Bailey, N. G. Busca, T. Delubac, J. Rich, É. Aubourg, J. E. Bautista, V. Bhardwaj, M. Blomqvist, A. S. Bolton, J. Bovy, J. Brownstein, B. Carithers, R. A. C. Croft, K. S. Dawson, A. Font-Ribera, J.-M. Le Goff, S. Ho, K. Honscheid, K.-G. Lee, D. Margala, P. McDonald, B. Medolin, J. Miralda-Escudé, A. D. Myers, R. C. Nichol, P. Noterdaeme, N. Palanque-Delabrouille, I. Pâris, P. Petitjean, M. M. Pieri, Y. Piškur, N. A. Roe, N. P. Ross, G. Rossi, D. J. Schlegel, D. P. Schneider, N. Suzuki, E. S. Sheldon, U. Seljak, M. Viel, D. H. Weinberg, and C. Yèche, *JCAP* **4**, 026 (2013), arXiv:1301.3459 [astro-ph.CO].
- [65] M. McQuinn and M. White, *Mon. Not. Roy. Astron. Soc.* **415**, 2257 (2011), arXiv:1102.1752 [astro-ph.CO].
- [66] V. Iršič, A. Slosar, S. Bailey, D. J. Eisenstein, A. Font-Ribera, J.-M. Le Goff, B. Lundgren, P. McDonald, R. O’Connell, N. Palanque-Delabrouille, P. Petitjean, J. Rich, G. Rossi, D. P. Schneider, E. S. Sheldon, and C. Yèche, ArXiv e-prints (2013), arXiv:1307.3403 [astro-ph.CO].
- [67] N. Palanque-Delabrouille, C. Yèche, A. Borde, J.-M. Le Goff, G. Rossi, M. Viel, É. Aubourg, S. Bailey, J. Bautista, M. Blomqvist, A. Bolton, J. S. Bolton, N. G. Busca, B. Carithers, R. A. C. Croft, K. S. Dawson, T. Delubac, A. Font-Ribera, S. Ho, D. Kirkby, K.-G. Lee, D. Margala, J. Miralda-Escudé, D. Muna, A. D. Myers, P. Noterdaeme, I. Pâris, P. Petitjean, M. M. Pieri, J. Rich, E. Rollinde, N. P. Ross, D. J. Schlegel, D. P. Schneider, A. Slosar, and D. H. Weinberg, ArXiv e-prints (2013), arXiv:1306.5896 [astro-ph.CO].
- [68] S. Bird, H. V. Peiris, M. Viel, and L. Verde, *Mon. Not. Roy. Astron. Soc.* **413**, 1717 (2011), arXiv:1010.1519 [astro-ph.CO].
- [69] N. Afshordi, G. Geshnizjani, and J. Khoury, *JCAP* **8**, 030 (2009), arXiv:0812.2244.
- [70] U. Seljak, A. Slosar, and P. McDonald, *Journal of Cosmology and Astro-Particle Physics* **10**, 14 (2006).
- [71] M. Viel, M. G. Haehnelt, and A. Lewis, *Mon. Not. Roy. Astron. Soc.* **370**, L51 (2006), arXiv:astro-ph/0604310.
- [72] A. Goobar, S. Hannestad, E. Mörtzell, and H. Tu, *JCAP* **6**, 019 (2006), arXiv:astro-ph/0602155.
- [73] U. Seljak, A. Makarov, P. McDonald, S. F. Anderson, N. A. Bahcall, J. Brinkmann, S. Burles, R. Cen, M. Doi, J. E. Gunn, Ž. Ivezić, S. Kent, J. Loveday, R. H. Lupton, J. A. Munn, R. C. Nichol, J. P. Ostriker, D. J. Schlegel, D. P. Schneider, M. Tegmark, D. E. Berk, D. H. Weinberg, and D. G. York, *Phys. Rev. D* **71**, 103515 (2005).
- [74] M. Viel, J. Lesgourgues, M. G. Haehnelt, S. Matarrese, and A. Riotto, *Phys. Rev. D* **71**, 063534 (2005).
- [75] S. Gratton, A. Lewis, and G. Efstathiou, *Phys. Rev. D* **77**, 083507 (2008), arXiv:0705.3100 [astro-ph].
- [76] P. McDonald, J. Miralda-Escudé, M. Rauch, W. L. W. Sargent, T. A. Barlow, and R. Cen, *Astrophys. J.* **562**, 52 (2001).
- [77] G. C. Rudie, C. C. Steidel, and M. Pettini, *Astrophys. J. Let.* **757**, L30 (2012), arXiv:1209.0005 [astro-ph.CO].
- [78] C.-A. Faucher-Giguère, J. X. Prochaska, A. Lidz, L. Hernquist, and M. Zaldarriaga, *Astrophys. J.* **681**, 831 (2008), arXiv:0709.2382.

- [79] P. McDonald, J. Miralda-Escudé, M. Rauch, W. L. W. Sargent, T. A. Barlow, R. Cen, and J. P. Ostriker, *Astrophys. J.* **543**, 1 (2000).
- [80] T. Kim, M. Viel, M. G. Haehnelt, R. F. Carswell, and S. Cristiani, *Mon. Not. Roy. Astron. Soc.* **347**, 355 (2004), arXiv:astro-ph/0308103.
- [81] P. McDonald, U. Seljak, R. Cen, D. Shih, D. H. Weinberg, S. Burles, D. P. Schneider, D. J. Schlegel, N. A. Bahcall, J. W. Briggs, J. Brinkmann, M. Fukugita, Ž. Ivezić, S. Kent, and D. E. Vanden Berk, *Astrophys. J.* **635**, 761 (2005).
- [82] P. McDonald, U. Seljak, R. Cen, P. Bode, and J. P. Ostriker, *Mon. Not. Roy. Astron. Soc.* **360**, 1471 (2005).
- [83] M. Viel and M. G. Haehnelt, *Mon. Not. Roy. Astron. Soc.* **365**, 231 (2006).
- [84] J. A. Regan, M. G. Haehnelt, and M. Viel, *Mon. Not. Roy. Astron. Soc.* **374**, 196 (2007), arXiv:astro-ph/0606638.
- [85] R. Mandelbaum, P. McDonald, U. Seljak, and R. Cen, *Mon. Not. Roy. Astron. Soc.* **344**, 776 (2003).
- [86] M. Viel, S. Matarrese, A. Heavens, M. G. Haehnelt, T.-S. Kim, V. Springel, and L. Hernquist, *Mon. Not. Roy. Astron. Soc.* **347**, L26 (2004).
- [87] A. Font-Ribera, E. Arnau, J. Miralda-Escudé, E. Rollinde, J. Brinkmann, J. R. Brownstein, K.-G. Lee, A. D. Myers, N. Palanque-Delabrouille, I. Pâris, P. Petitjean, J. Rich, N. P. Ross, D. P. Schneider, and M. White, *JCAP* **5**, 018 (2013), arXiv:1303.1937 [astro-ph.CO].
- [88] N. Hamaus, U. Seljak, V. Desjacques, R. E. Smith, and T. Baldauf, *Phys. Rev. D* **82**, 043515 (2010), arXiv:1004.5377 [astro-ph.CO].
- [89] N. Hamaus, U. Seljak, and V. Desjacques, *Phys. Rev. D* **86**, 103513 (2012), arXiv:1207.1102 [astro-ph.CO].
- [90] U. Seljak, N. Hamaus, and V. Desjacques, *Physical Review Letters* **103**, 091303 (2009), arXiv:0904.2963 [astro-ph.CO].
- [91] K. S. Dawson, D. J. Schlegel, C. P. Ahn, S. F. Anderson, É. Aubourg, S. Bailey, R. H. Barkhouser, J. E. Bautista, A. Beifiori, A. A. Berlind, V. Bhardwaj, D. Bizyaev, C. H. Blake, M. R. Blanton, M. Blomqvist, A. S. Bolton, A. Borde, J. Bovy, W. N. Brandt, H. Brewington, J. Brinkmann, P. J. Brown, J. R. Brownstein, K. Bundy, N. G. Busca, W. Carithers, A. R. Carnero, M. A. Carr, Y. Chen, J. Comparat, N. Connolly, F. Cope, R. A. C. Croft, A. J. Cuesta, L. N. da Costa, J. R. A. Davenport, T. Delubac, R. de Putter, S. Dhital, A. Ealet, G. L. Ebelke, D. J. Eisenstein, S. Escoffier, X. Fan, N. Filiz Ak, H. Finley, A. Font-Ribera, R. Génova-Santos, J. E. Gunn, H. Guo, D. Haggard, P. B. Hall, J.-C. Hamilton, B. Harris, D. W. Harris, S. Ho, D. W. Hogg, D. Holder, K. Honscheid, J. Huehnerhoff, B. Jordan, W. P. Jordan, G. Kauffmann, E. A. Kazin, D. Kirkby, M. A. Klaene, J.-P. Kneib, J.-M. Le Goff, K.-G. Lee, D. C. Long, C. P. Loomis, B. Lundgren, R. H. Lupton, M. A. G. Maia, M. Makler, E. Malanushenko, V. Malanushenko, R. Mandelbaum, M. Manera, C. Maraston, D. Margala, K. L. Masters, C. K. McBride, P. McDonald, I. D. McGreer, R. G. McMahon, O. Mena, J. Miralda-Escudé, A. D. Montero-Dorta, F. Montesano, D. Muna, A. D. Myers, T. Naugle, R. C. Nichol, P. Noterdaeme, S. E. Nuza, M. D. Olmstead, A. Oravetz, D. J. Oravetz, R. Owen, N. Padmanabhan, N. Palanque-Delabrouille, K. Pan, J. K. Parejko, I. Pâris, W. J. Percival, I. Pérez-Fournon, I. Pérez-Ràfols, P. Petitjean, R. Pfaffenberger, J. Pforr, M. M. Pieri, F. Prada, A. M. Price-Whelan, M. J. Raddick, R. Rebolo, J. Rich, G. T. Richards, C. M. Rockosi, N. A. Roe, A. J. Ross, N. P. Ross, G. Rossi, J. A. Rubiño-Martín, L. Samushia, A. G. Sánchez, C. Sayres, S. J. Schmidt, D. P. Schneider, C. G. Scóccola, H.-J. Seo, A. Shelden, E. Sheldon, Y. Shen, Y. Shu, A. Slosar, S. A. Smee, S. A. Snedden, F. Stauffer, O. Steele, M. A. Strauss, A. Streblyanska, N. Suzuki, M. E. C. Swanson, T. Tal, M. Tanaka, D. Thomas, J. L. Tinker, R. Tojeiro, C. A. Tremonti, M. Vargas Magaña, L. Verde, M. Viel, D. A. Wake, M. Watson, B. A. Weaver, D. H. Weinberg, B. J. Weiner, A. A. West, M. White, W. M. Wood-Vasey, C. Yèche, I. Zehavi, G.-B. Zhao, and Z. Zheng, *AJ* **145**, 10 (2013), arXiv:1208.0022 [astro-ph.CO].
- [92] B. A. Reid, L. Samushia, M. White, W. J. Percival, M. Manera, N. Padmanabhan, A. J. Ross, A. G. Sánchez, S. Bailey, D. Bizyaev, A. S. Bolton, H. Brewington, J. Brinkmann, J. R. Brownstein, A. J. Cuesta, D. J. Eisenstein, J. E. Gunn, K. Honscheid, E. Malanushenko, V. Malanushenko, C. Maraston, C. K. McBride, D. Muna, R. C. Nichol, D. Oravetz, K. Pan, R. de Putter, N. A. Roe, N. P. Ross, D. J. Schlegel, D. P. Schneider, H.-J. Seo, A. Shelden, E. S. Sheldon, A. Simmons, R. A. Skibba, S. Snedden, M. E. C. Swanson, D. Thomas, J. Tinker, R. Tojeiro, L. Verde, D. A. Wake, B. A. Weaver, D. H. Weinberg, I. Zehavi, and G.-B. Zhao, *Mon. Not. Roy. Astron. Soc.* **426**, 2719 (2012), arXiv:1203.6641 [astro-ph.CO].
- [93] L. Jiang, X. Fan, R. J. Cool, D. J. Eisenstein, I. Zehavi, G. T. Richards, R. Scranton, D. Johnston, M. A. Strauss, D. P. Schneider, and J. Brinkmann, *AJ* **131**, 2788 (2006), arXiv:astro-ph/0602569.
- [94] L. Anderson, E. Aubourg, S. Bailey, D. Bizyaev, M. Blanton, A. S. Bolton, J. Brinkmann, J. R. Brownstein, A. Burden, A. J. Cuesta, L. A. N. da Costa, K. S. Dawson, R. de Putter, D. J. Eisenstein, J. E. Gunn, H. Guo, J.-C. Hamilton, P. Harding, S. Ho, K. Honscheid, E. Kazin, D. Kirkby, J.-P. Kneib, A. Labatie, C. Loomis, R. H. Lupton, E. Malanushenko, V. Malanushenko, R. Mandelbaum, M. Manera, C. Maraston, C. K. McBride, K. T. Mehta, O. Mena, F. Montesano, D. Muna, R. C. Nichol, S. E. Nuza, M. D. Olmstead, D. Oravetz, N. Padmanabhan, N. Palanque-Delabrouille, K. Pan, J. Parejko, I. Pâris, W. J. Percival, P. Petitjean, F. Prada, B. Reid, N. A. Roe, A. J. Ross, N. P. Ross, L. Samushia, A. G. Sánchez, D. J. Schlegel, D. P. Schneider, C. G. Scóccola, H.-J. Seo, E. S. Sheldon, A. Simmons, R. A. Skibba, M. A. Strauss, M. E. C. Swanson, D. Thomas, J. L. Tinker, R. Tojeiro, M. V. Magaña, L. Verde, C. Wagner, D. A. Wake, B. A. Weaver, D. H. Weinberg, M. White, X. Xu, C. Yèche, I. Zehavi, and G.-B. Zhao, *Mon. Not. Roy. Astron. Soc.* **427**, 3435 (2012), arXiv:1203.6594 [astro-ph.CO].
- [95] R. Takahashi, N. Yoshida, M. Takada, T. Matsubara, N. Sugiyama, I. Kayo, A. J. Nishizawa, T. Nishimichi, S. Saito, and A. Taruya, *Astrophys. J.* **700**, 479 (2009), arXiv:0902.0371 [astro-ph.CO].
- [96] B. A. Reid and M. White, *Mon. Not. Roy. Astron. Soc.* **417**, 1913 (2011), arXiv:1105.4165 [astro-ph.CO].
- [97] G. e. a. Zhao, “The Extended BOSS Survey (eBOSS),” , in preparation (2013).
- [98] C.-T. Chiang, P. Wullstein, D. Jeong, E. Komatsu, G. A. Blanc, R. Ciardullo, N. Drory, M. Fabricius, S. Finkelstein,

- K. Gebhardt, C. Gronwall, A. Hagen, G. J. Hill, S. Jogee, M. Landriau, E. Mentuch Cooper, D. P. Schneider, and S. Tuttle, ArXiv e-prints (2013), arXiv:1306.4157 [astro-ph.CO].
- [99] M. Levi, C. Bebek, T. Beers, R. Blum, R. Cahn, D. Eisenstein, B. Flaugher, K. Honscheid, R. Kron, O. Lahav, P. McDonald, N. Roe, D. Schlegel, and representing the DESI collaboration, ArXiv e-prints (2013), arXiv:1308.0847 [astro-ph.CO].
- [100] D. Schlegel, F. Abdalla, T. Abraham, C. Ahn, C. Allende Prieto, J. Annis, E. Aubourg, M. Azzaro, S. B. C. Baltay, C. Baugh, C. Bebek, S. Becerril, M. Blanton, A. Bolton, B. Bromley, R. Cahn, P. . Carton, J. L. Cervantes-Cota, Y. Chu, M. Cortes, K. Dawson, A. Dey, M. Dickinson, H. T. Diehl, P. Doel, A. Ealet, J. Edelman, D. Eppelle, S. Escoffier, A. Evrard, L. Faccioli, C. Frenk, M. Geha, D. Gerdes, P. Gondolo, A. Gonzalez-Arroyo, B. Grossan, T. Heckman, H. Heetderks, S. Ho, K. Honscheid, D. Huterer, O. Ilbert, I. Ivans, P. Jelinsky, Y. Jing, D. Joyce, R. Kennedy, S. Kent, D. Kieda, A. Kim, C. Kim, J. . Kneib, X. Kong, A. Kosowsky, K. Krishnan, O. Lahav, M. Lampton, S. LeBohec, V. Le Brun, M. Levi, C. Li, M. Liang, H. Lim, W. Lin, E. Linder, W. Lorenzon, A. de la Macorra, C. Magneville, R. Malina, C. Marinoni, V. Martinez, S. Majewski, T. Matheson, R. McCloskey, P. McDonald, T. McKay, J. McMahon, B. Menard, J. Miralda-Escude, M. Modjaz, A. Montero-Dorta, I. Morales, N. Mostek, J. Newman, R. Nichol, P. Nugent, K. Olsen, N. Padmanabhan, N. Palanque-Delabrouille, I. Park, J. Peacock, W. Percival, S. Perlmutter, C. Peroux, P. Petitjean, F. Prada, E. Prieto, J. Prochaska, K. Reil, C. Rockosi, N. Roe, E. Rollinde, A. Roodman, N. Ross, G. Rudnick, V. Ruhlmann-Kleider, J. Sanchez, D. Sawyer, C. Schimd, M. Schubnell, R. Scoccimaro, U. Seljak, H. Seo, E. Sheldon, M. Sholl, R. Shulte-Ladbeck, A. Slosar, D. S. Smith, G. Smoot, W. Springer, A. Stril, A. S. Szalay, C. Tao, G. Tarle, E. Taylor, A. Tilquin, J. Tinker, F. Valdes, J. Wang, T. Wang, B. A. Weaver, D. Weinberg, M. White, M. Wood-Vasey, J. Yang, X. Y. C. Yeche, N. Zakamska, A. Zentner, C. Zhai, and P. Zhang, ArXiv e-prints (2011), arXiv:1106.1706 [astro-ph.IM].
- [101] N. Mostek, K. Barbary, C. J. Bebek, A. T. Dey, J. Edelman, P. Jelinsky, A. G. Kim, M. L. Lampton, M. E. Levi, P. McDonald, C. Poppett, N. A. Roe, D. J. Schlegel, and M. J. Sholl, in *Society of Photo-Optical Instrumentation Engineers (SPIE) Conference Series*, Society of Photo-Optical Instrumentation Engineers (SPIE) Conference Series, Vol. 8446 (2012).
- [102] N. J. Mostek, K. Barbary, A. Dey, R. Kennedy, A. Kim, J. Kneib, J. Newman, P. Nugent, N. Padmanabhan, D. Schlegel, and BigBOSS Collaboration, in *American Astronomical Society Meeting Abstracts #219*, American Astronomical Society Meeting Abstracts, Vol. 219 (2012) p. #335.13.
- [103] N. Mostek, A. L. Coil, M. Cooper, M. Davis, J. A. Newman, and B. J. Weiner, *Astrophys. J.* **767**, 89 (2013), arXiv:1210.6694 [astro-ph.CO].
- [104] N. P. Ross, Y. Shen, M. A. Strauss, D. E. Vanden Berk, A. J. Connolly, G. T. Richards, D. P. Schneider, D. H. Weinberg, P. B. Hall, N. A. Bahcall, and R. J. Brunner, *Astrophys. J.* **697**, 1634 (2009), arXiv:0903.3230 [astro-ph.CO].
- [105] N. Palanque-Delabrouille, C. Magneville, C. Yèche, S. Eftekharzadeh, A. D. Myers, P. Petitjean, I. Pâris, E. Aubourg, I. McGreer, X. Fan, A. Dey, D. Schlegel, S. Bailey, D. Bizayev, A. Bolton, K. Dawson, G. Ebelke, J. Ge, E. Malanushenko, V. Malanushenko, D. Oravetz, K. Pan, N. P. Ross, D. P. Schneider, E. Sheldon, A. Simmons, J. Tinker, M. White, and C. Willmer, *Astron. Astrophys.* **551**, A29 (2013), arXiv:1209.3968 [astro-ph.CO].
- [106] R. Laureijs, J. Amiaux, S. Arduini, J. . Auguères, J. Brinchmann, R. Cole, M. Cropper, C. Dabin, L. Duvet, A. Ealet, and et al., ArXiv e-prints (2011), arXiv:1110.3193 [astro-ph.CO].
- [107] D. Spergel, N. Gehrels, J. Breckinridge, M. Donahue, A. Dressler, B. S. Gaudi, T. Greene, O. Guyon, C. Hirata, J. Kalirai, N. J. Kasdin, W. Moos, S. Perlmutter, M. Postman, B. Rauscher, J. Rhodes, Y. Wang, D. Weinberg, J. Centrella, W. Traub, C. Baltay, J. Colbert, D. Bennett, A. Kiessling, B. Macintosh, J. Merten, M. Mortonson, M. Penny, E. Rozo, D. Savransky, K. Stapelfeldt, Y. Zu, C. Baker, E. Cheng, D. Content, J. Dooley, M. Foote, R. Goulioud, K. Grady, C. Jackson, J. Kruk, M. Levine, M. Melton, C. Peddie, J. Ruffa, and S. Shaklan, ArXiv e-prints (2013), arXiv:1305.5422 [astro-ph.IM].
- [108] R. Nakajima, R. Mandelbaum, U. Seljak, J. D. Cohn, R. Reyes, and R. Cool, *Mon. Not. Roy. Astron. Soc.* **420**, 3240 (2012), arXiv:1107.1395 [astro-ph.CO].
- [109] J. Yoo and U. Seljak, *Phys. Rev. D* **86**, 083504 (2012), arXiv:1207.2471 [astro-ph.CO].
- [110] M. Sato, T. Hamana, R. Takahashi, M. Takada, N. Yoshida, T. Matsubara, and N. Sugiyama, *Astrophys. J.* **701**, 945 (2009), arXiv:0906.2237 [astro-ph.CO].
- [111] A. Cooray and W. Hu, *Astrophys. J.* **554**, 56 (2001), arXiv:astro-ph/0012087.
- [112] J. Guzik, B. Jain, and M. Takada, *Phys. Rev. D* **81**, 023503 (2010), arXiv:0906.2221 [astro-ph.CO].
- [113] W. Hu and B. Jain, *Phys. Rev. D* **70**, 043009 (2004), arXiv:astro-ph/0312395.
- [114] P. McDonald, H. Trac, and C. Contaldi, *Mon. Not. Roy. Astron. Soc.* **366**, 547 (2006).
- [115] R. E. Smith, J. A. Peacock, A. Jenkins, S. D. M. White, C. S. Frenk, F. R. Pearce, P. A. Thomas, G. Efstathiou, and H. M. P. Couchman, *Mon. Not. Roy. Astron. Soc.* **341**, 1311 (2003).
- [116] C. Ma, *Astrophys. J. Let.* **508**, L5 (1998).
- [117] A. P. Hearin, A. R. Zentner, and Z. Ma, *JCAP* **4**, 034 (2012), arXiv:1111.0052 [astro-ph.CO].
- [118] G. Bernstein and D. Huterer, *Mon. Not. Roy. Astron. Soc.* **401**, 1399 (2010), arXiv:0902.2782 [astro-ph.CO].
- [119] P. Zhang, U.-L. Pen, and G. Bernstein, *Mon. Not. Roy. Astron. Soc.* **405**, 359 (2010), arXiv:0910.4181 [astro-ph.CO].
- [120] J. A. Newman, *Astrophys. J.* **684**, 88 (2008), arXiv:0805.1409.
- [121] Z. Ma and G. Bernstein, *Astrophys. J.* **682**, 39 (2008), arXiv:0712.1562.
- [122] Z. Ma, W. Hu, and D. Huterer, *Astrophys. J.* **636**, 21 (2006), arXiv:astro-ph/0506614.
- [123] LSST Science Collaboration, P. A. Abell, J. Allison, S. F. Anderson, J. R. Andrew, J. R. P. Angel, L. Armus, D. Arnett, S. J. Asztalos, T. S. Axelrod, and et al., ArXiv e-prints (2009), arXiv:0912.0201 [astro-ph.IM].
- [124] J. Lesgourgues and S. Pastor, ArXiv e-prints (2012), arXiv:1212.6154 [hep-ph].

- [125] C. Carbone, Nuclear Physics B Proceedings Supplements **237**, 50 (2013).
- [126] L. Santos, P. Cabella, A. Balbi, and N. Vittorio, ArXiv e-prints (2013), arXiv:1307.2919 [astro-ph.CO].
- [127] J. Hamann, S. Hannestad, and Y. Y. Y. Wong, JCAP **11**, 052 (2012), arXiv:1209.1043 [astro-ph.CO].
- [128] M. Costanzi Alunno Cerbolini, B. Sartoris, J.-Q. Xia, A. Biviano, S. Borgani, and M. Viel, JCAP **6**, 020 (2013), arXiv:1303.4550 [astro-ph.CO].
- [129] T. Basse, O. Eggers Bjaelde, J. Hamann, S. Hannestad, and Y. Y. Y. Wong, ArXiv e-prints (2013), arXiv:1304.2321 [astro-ph.CO].
- [130] Y. Oyama, A. Shimizu, and K. Kohri, Physics Letters B **718**, 1186 (2013), arXiv:1205.5223 [astro-ph.CO].
- [131] A. C. Hall and A. Challinor, *Mon. Not. Roy. Astron. Soc.* **425**, 1170 (2012), arXiv:1205.6172 [astro-ph.CO].
- [132] S. Joudaki and M. Kaplinghat, Phys. Rev. D **86**, 023526 (2012), arXiv:1106.0299 [astro-ph.CO].
- [133] R. N. Cahn, D. A. Dwyer, S. J. Freedman, W. C. Haxton, R. W. Kadel, Y. G. Kolomensky, K. B. Luk, P. McDonald, G. D. Orebi Gann, and A. W. P. Poon, ArXiv e-prints (2013), arXiv:1307.5487 [hep-ex].
- [134] A. Slosar, P. McDonald, and BigBOSS Team, in *American Astronomical Society Meeting Abstracts #219*, American Astronomical Society Meeting Abstracts, Vol. 219 (2012) p. #335.01.
- [135] A. Slosar, Phys. Rev. D **73**, 123501 (2006), arXiv:astro-ph/0602133.
- [136] R. Jimenez, T. Kitching, C. Peña-Garay, and L. Verde, JCAP **5**, 035 (2010), arXiv:1003.5918 [astro-ph.CO].
- [137] C. Wagner, L. Verde, and R. Jimenez, *Astrophys. J. Let.* **752**, L31 (2012), arXiv:1203.5342 [astro-ph.CO].
- [138] F. de Bernardis, T. D. Kitching, A. Heavens, and A. Melchiorri, Phys. Rev. D **80**, 123509 (2009), arXiv:0907.1917 [astro-ph.CO].
- [139] J. Beringer, J.-F. Arguin, R. M. Barnett, K. Copic, O. Dahl, D. E. Groom, C.-J. Lin, J. Lys, H. Murayama, C. G. Wohl, W.-M. Yao, P. A. Zyla, C. Amsler, M. Antonelli, D. M. Asner, H. Baer, H. R. Band, T. Basaglia, C. W. Bauer, J. J. Beatty, V. I. Belousov, E. Bergren, G. Bernardi, W. Bertl, S. Bethke, H. Bichsel, O. Biebel, E. Blucher, S. Blusk, G. Brooijmans, O. Buchmueller, R. N. Cahn, M. Carena, A. Ceccucci, D. Chakraborty, M.-C. Chen, R. S. Chivukula, G. Cowan, G. D'Ambrosio, T. Damour, D. de Florian, A. de Gouvêa, T. DeGrand, P. de Jong, G. Dissertori, B. Dobrescu, M. Doser, M. Drees, D. A. Edwards, S. Eidelman, J. Erler, V. V. Ezhela, W. Fetscher, B. D. Fields, B. Foster, T. K. Gaisser, L. Garren, H.-J. Gerber, G. Gerbier, T. Gherghetta, S. Golwala, M. Goodman, C. Grab, A. V. Gritsan, J.-F. Grivaz, M. Grünwald, A. Gurtu, T. Gutsche, H. E. Haber, K. Hagiwara, C. Hagmann, C. Hanhart, S. Hashimoto, K. G. Hayes, M. Heffner, B. Heltsley, J. J. Hernández-Rey, K. Hikasa, A. Höcker, J. Holder, A. Holtkamp, J. Huston, J. D. Jackson, K. F. Johnson, T. Junk, D. Karlen, D. Kirkby, S. R. Klein, E. Klempt, R. V. Kowalewski, F. Krauss, M. Kreps, B. Krusche, Y. V. Kuyanov, Y. Kwon, O. Lahav, J. Laiho, P. Langacker, A. Liddle, Z. Ligeti, T. M. Liss, L. Littenberg, K. S. Lugovsky, S. B. Lugovsky, T. Mannel, A. V. Manohar, W. J. Marciano, A. D. Martin, A. Masoni, J. Matthews, D. Milstead, R. Miquel, K. Mönig, F. Moortgat, K. Nakamura, M. Narain, P. Nason, S. Navas, M. Neubert, P. Nevski, Y. Nir, K. A. Olive, L. Pape, J. Parsons, C. Patrignani, J. A. Peacock, S. T. Petcov, A. Piepke, A. Pomarol, G. Punzi, A. Quadt, S. Raby, G. Raffelt, B. N. Ratcliff, P. Richardson, S. Roesler, S. Rolli, A. Romaniouk, L. J. Rosenberg, J. L. Rosner, C. T. Sachrajda, Y. Sakai, G. P. Salam, S. Sarkar, F. Sauli, O. Schneider, K. Scholberg, D. Scott, W. G. Seligman, M. H. Shaevitz, S. R. Sharpe, M. Silari, T. Sjöstrand, P. Skands, J. G. Smith, G. F. Smoot, S. Spanier, H. Spieler, A. Stahl, T. Stanev, S. L. Stone, T. Sumiyoshi, M. J. Syphers, F. Takahashi, M. Tanabashi, J. Terning, M. Titov, N. P. Tkachenko, N. A. Törnqvist, D. Tovey, G. Valencia, K. van Bibber, G. Venanzoni, M. G. Vincter, P. Vogel, A. Vogt, W. Walkowiak, C. W. Walter, D. R. Ward, T. Watari, G. Weiglein, E. J. Weinberg, L. R. Wiencke, L. Wolfenstein, J. Womersley, C. L. Woody, R. L. Workman, A. Yamamoto, G. P. Zeller, O. V. Zenin, J. Zhang, R.-Y. Zhu, G. Harper, V. S. Lugovsky, and P. Schaffner, Phys. Rev. D **86**, 010001 (2012).
- [140] A. Albrecht, G. Bernstein, R. Cahn, W. L. Freedman, J. Hewitt, W. Hu, J. Huth, M. Kamionkowski, E. W. Kolb, L. Knox, J. C. Mather, S. Staggs, and N. B. Suntzeff, ArXiv Astrophysics e-prints (2006), astro-ph/0609591.
- [141] P. McDonald, Phys. Rev. D **78**, 123519 (2008), arXiv:0806.1061.
- [142] Planck Collaboration, P. A. R. Ade, N. Aghanim, C. Armitage-Caplan, M. Arnaud, M. Ashdown, F. Atrio-Barandela, J. Aumont, C. Baccigalupi, A. J. Banday, and et al., ArXiv e-prints (2013), arXiv:1303.5084 [astro-ph.CO].
- [143] E. Sefusatti, M. Crocce, and V. Desjacques, *Mon. Not. Roy. Astron. Soc.* **425**, 2903 (2012), arXiv:1111.6966 [astro-ph.CO].
- [144] T. Baldauf, U. Seljak, and L. Senatore, JCAP **4**, 006 (2011), arXiv:1011.1513 [astro-ph.CO].
- [145] T. Nishimichi, A. Taruya, K. Koyama, and C. Sabiu, JCAP **7**, 002 (2010), arXiv:0911.4768 [astro-ph.CO].
- [146] M. Liguori, E. Sefusatti, J. R. Fergusson, and E. P. S. Shellard, *Advances in Astronomy* **2010**, 980523 (2010), 10.1155/2010/980523, arXiv:1001.4707 [astro-ph.CO].
- [147] E. Sefusatti, Phys. Rev. D **80**, 123002 (2009), arXiv:0905.0717 [astro-ph.CO].
- [148] D. Jeong and E. Komatsu, *Astrophys. J.* **703**, 1230 (2009), arXiv:0904.0497 [astro-ph.CO].
- [149] T. L. Smith, S. Das, and O. Zahn, Phys. Rev. D **85**, 023001 (2012), arXiv:1105.3246 [astro-ph.CO].
- [150] Z. Hou, R. Keisler, L. Knox, M. Millea, and C. Reichardt, Phys. Rev. D **87**, 083008 (2013), arXiv:1104.2333 [astro-ph.CO].
- [151] C. Brust, D. E. Kaplan, and M. T. Walters, ArXiv e-prints (2013), arXiv:1303.5379 [hep-ph].
- [152] C. Boehm, M. J. Dolan, and C. McCabe, JCAP **12**, 027 (2012), arXiv:1207.0497 [astro-ph.CO].
- [153] M. Wyman, D. H. Rudd, R. A. Vanderveld, and W. Hu, ArXiv e-prints (2013), arXiv:1307.7715 [astro-ph.CO].
- [154] R. de Putter, O. Zahn, and E. V. Linder, Phys. Rev. D **79**, 065033 (2009), arXiv:0901.0916 [astro-ph.CO].
- [155] R. Hlozek, J. Dunkley, G. Addison, J. W. Appel, J. R. Bond, C. Sofia Carvalho, S. Das, M. J. Devlin, R. Dünner, T. Essinger-Hileman, J. W. Fowler, P. Gallardo, A. Hajian, M. Halpern, M. Hasselfield, M. Hilton, A. D. Hincks, J. P. Hughes, K. D. Irwin, J. Klein, A. Kosowsky, T. A. Marriage, D. Marsden, F. Menanteau, K. Moodley, M. D. Niemack, M. R. Nolta, L. A. Page, L. Parker, B. Partridge, F. Rojas, N. Sehgal, B. Sherwin, J. Sievers, D. N. Spergel, S. T. Staggs,

- D. S. Swetz, E. R. Switzer, R. Thornton, and E. Wollack, *Astrophys. J.* **749**, 90 (2012), arXiv:1105.4887 [astro-ph.CO].
- [156] T.-C. Chang, U.-L. Pen, J. B. Peterson, and P. McDonald, *Physical Review Letters* **100**, 091303 (2008), arXiv:0709.3672.
- [157] J. C. Pober, A. R. Parsons, D. R. DeBoer, P. McDonald, M. McQuinn, J. E. Aguirre, Z. Ali, R. F. Bradley, T.-C. Chang, and M. F. Morales, *AJ* **145**, 65 (2013), arXiv:1210.2413 [astro-ph.CO].
- [158] K. W. Masui, P. McDonald, and U. Pen, *Phys. Rev. D* **81**, 103527 (2010), arXiv:1001.4811 [astro-ph.CO].
- [159] M. Tegmark and M. Zaldarriaga, *Phys. Rev. D* **82**, 103501 (2010), arXiv:0909.0001 [astro-ph.CO].
- [160] K. W. Masui, F. Schmidt, U. Pen, and P. McDonald, *Phys. Rev. D* **81**, 062001 (2010), arXiv:0911.3552.
- [161] V. Desjacques and U. Seljak, *Advances in Astronomy* **2010**, 908640 (2010), 10.1155/2010/908640, arXiv:1006.4763 [astro-ph.CO].
- [162] D. Tseliakhovich, C. Hirata, and A. Slosar, *Phys. Rev. D* **82**, 043531 (2010), arXiv:1004.3302 [astro-ph.CO].
- [163] V. Desjacques and U. Seljak, *Phys. Rev. D* **81**, 023006 (2010), arXiv:0907.2257 [astro-ph.CO].
- [164] C. Wagner, L. Verde, and L. Boubekeur, *JCAP* **10**, 022 (2010), arXiv:1006.5793 [astro-ph.CO].
- [165] N. Barnaby, *Phys. Rev. D* **82**, 106009 (2010), arXiv:1006.4615 [astro-ph.CO].
- [166] A. Becker, D. Huterer, and K. Kadota, *JCAP* **1**, 006 (2011), arXiv:1009.4189 [astro-ph.CO].
- [167] M. LoVerde and K. M. Smith, *JCAP* **8**, 003 (2011), arXiv:1102.1439 [astro-ph.CO].
- [168] K. M. Smith and M. LoVerde, *JCAP* **11**, 009 (2011), arXiv:1010.0055 [astro-ph.CO].
- [169] C. Wagner and L. Verde, *JCAP* **3**, 002 (2012), arXiv:1102.3229 [astro-ph.CO].
- [170] R. Scoccimarro, L. Hui, M. Manera, and K. C. Chan, *Phys. Rev. D* **85**, 083002 (2012), arXiv:1108.5512 [astro-ph.CO].
- [171] E. Sefusatti, J. R. Fergusson, X. Chen, and E. P. S. Shellard, *JCAP* **8**, 033 (2012), arXiv:1204.6318 [astro-ph.CO].
- [172] M. Biagetti, V. Desjacques, and A. Riotto, *Mon. Not. Roy. Astron. Soc.* **429**, 1774 (2013), arXiv:1208.1616 [astro-ph.CO].
- [173] E. Nelson and S. Shandera, *Physical Review Letters* **110**, 131301 (2013), arXiv:1212.4550 [astro-ph.CO].
- [174] N. Barnaby and Z. Huang, *Phys. Rev. D* **80**, 126018 (2009), arXiv:0909.0751 [astro-ph.CO].
- [175] E. Sefusatti, M. Liguori, A. P. S. Yadav, M. G. Jackson, and E. Pajer, *JCAP* **12**, 022 (2009), arXiv:0906.0232 [astro-ph.CO].
- [176] M. Kawasaki, K. Nakayama, T. Sekiguchi, T. Suyama, and F. Takahashi, *JCAP* **1**, 042 (2009), arXiv:0810.0208.
- [177] M. Kawasaki, K. Nakayama, and F. Takahashi, *JCAP* **1**, 026 (2009), arXiv:0810.1585 [hep-ph].
- [178] M. Viel, G. D. Becker, J. S. Bolton, and M. G. Haehnelt, *ArXiv e-prints* (2013), arXiv:1306.2314 [astro-ph.CO].
- [179] M. Viel, G. D. Becker, J. S. Bolton, M. G. Haehnelt, M. Rauch, and W. L. W. Sargent, *Physical Review Letters* **100**, 041304 (2008), arXiv:0709.0131.
- [180] U. Seljak, A. Makarov, P. McDonald, and H. Trac, *Physical Review Letters* **97**, 191303 (2006).
- [181] N. Afshordi, P. McDonald, and D. N. Spergel, *Astrophys. J. Let.* **594**, L71 (2003).
- [182] B. J. Carr, K. Kohri, Y. Sendouda, and J. Yokoyama, *Phys. Rev. D* **81**, 104019 (2010), arXiv:0912.5297 [astro-ph.CO].
- [183] E. Krause and C. M. Hirata, *Mon. Not. Roy. Astron. Soc.* **410**, 2730 (2011), arXiv:1004.3611 [astro-ph.CO].
- [184] C. M. Hirata, *Mon. Not. Roy. Astron. Soc.* **399**, 1074 (2009), arXiv:0903.4929.
- [185] E. Gaztañaga, M. Eriksen, M. Crocce, F. J. Castander, P. Fosalba, P. Marti, R. Miquel, and A. Cabré, *Mon. Not. Roy. Astron. Soc.* **422**, 2904 (2012), arXiv:1109.4852 [astro-ph.CO].
- [186] D. Kirk, O. Lahav, S. Bridle, S. Jouvel, F. B. Abdalla, and J. A. Frieman, *ArXiv e-prints* (2013), arXiv:1307.8062 [astro-ph.CO].
- [187] R. de Putter, O. Doré, and S. Das, *ArXiv e-prints* (2013), arXiv:1306.0534 [astro-ph.CO].
- [188] Y.-C. Cai and G. Bernstein, *Mon. Not. Roy. Astron. Soc.* **422**, 1045 (2012), arXiv:1112.4478 [astro-ph.CO].

VIII. APPENDIX

A. Traditional FoM without neutrino masses

For comparison to past work, Table XXIII shows traditional FoMs with fixed neutrino mass.

Table XXV shows traditional FoMs based on FoMSWG parameters and the FoMSWG Planck Fisher matrix.

We see by comparing these two tables that our treatment of Planck gives very similar results to the FoMSWG treatment (they are not intended to be identical – e.g., we use a different parameter set and do not assume the τ measurement will be systematics limited). On the other hand, our treatment of DES is quite optimistic relative to the FoMSWG Stage III weak lensing example (we do not include shear calibration uncertainty, intrinsic alignments, etc.).

B. Overlapping redshift and photometric surveys

It has been suggested that dramatic gains in constraining power can be achieved when redshift surveys and photometric (lensing) surveys overlap on the sky [185], so they can be directly cross-correlated rather than simply providing complementary parameter constraints. We investigated this possibility but did not find significant gains, so we left it out of our main discussion for simplicity. We may address this in detail in a future paper, but, because it might be

expected that this would be a big part of parameter projections like ours, we give some basic results and discussion here. (The authors of [185] did find some problems with their calculations (E. Gaztanaga, private communication), although the issue has not been entirely resolved.)

1. Overlapping survey Fisher matrices

We compute Fisher matrices for overlapping surveys by first treating the redshift survey galaxies as more angular clustering tracers, with zero photo- z errors, for the purpose of cross-correlations, and then adding a standard 3D power spectrum-based redshift survey Fisher matrix to pick up the small-radial-scale information. Ideally, the auto angular clustering at different redshifts and cross-correlation between them has the same information as the 3D power spectrum. We use 3D power Fisher matrices at small scales because the angular clustering is evaluated using a wide redshift bin, i.e., $\Delta z = 0.2$ is used and the 3D Fisher matrix is added to account for radial information internal to the $\Delta z = 0.2$ slice (it is unnecessarily computationally cumbersome to try to fully resolve the redshift survey information by making Δz very small, e.g., bins of width $\Delta z \sim 0.001(1+z)$ are required to resolve the BAO feature). In order to avoid double-counting very low k_z information which is already included in the angular correlations, we down-weight 3D redshift-survey modes in overlapping calculations by a factor $1 - [\sin(f_{k_z} k_z \Delta z) / (f_{k_z} k_z \Delta z)]^2$, where Δz is the width of the angular clustering bins. This damping factor, which cannot be derived rigorously, was calibrated, finding $f_{k_z} = 1$, by the requirement that, when using only redshift survey galaxies, Fisher matrix results computed in purely redshift-survey (3D power spectrum) mode were the same as the summed Fisher matrix results from redshift-survey mode on small radial scales and angular clustering mode on large radial scales. The exact value of f_{k_z} is unimportant, however, because in the end this is only a tiny fraction of redshift survey modes, as we discuss below.

Results possibly including overlapping LSST and DESI are shown in Table XXVII. While the redshift and lensing surveys are highly complementary, whether they overlap or not makes very little difference. To verify that this conclusion is not sensitive to our redshift binning, we show results for both $\Delta z = 0.2$ and $\Delta z = 0.1$. The biggest difference is that the FoM for Planck+LSST improves by 20% for the finer binning, presumably because $\Delta z = 0.2$ bins are still wider than our assumed $0.05(1+z)$ rms photo- z errors, so some information is lost. The few percent degradation of the redshift survey with finer binning is presumably due to the extra free bias parameters introduced. In any case, the most relevant combined results change by less than 10%, and the gain from overlap is almost the same.

Note that this calculation is not directly comparable to [186] because they compute their spectroscopic survey constraint using exclusively a C_ℓ method like we use for the photometric constraints, with bins of width $\Delta z = 0.05$, corresponding to $\sim 85 h^{-1}\text{Mpc}$ at $z \sim 1$ – clearly far from what is necessary to resolve the BAO-scale structure where we find the bulk of our redshift survey information. There are a lot of other differences, e.g., they generally do not include Planck constraints, and do not include correlations involving photometric galaxy density (i.e., autocorrelations and what is usually called galaxy-galaxy lensing), which enhance the constraining power of the non-overlapping case. Our conclusion is consistent with [187], who find gains in certain scenarios including photo- z systematic uncertainties, but not in our scenario.

2. Qualitative understanding of why cross-correlations are not very helpful

Given the intuitive appeal of overlapping lensing and redshift surveys, and the results of [185], some further effort to qualitatively understand the results here seems desirable. ([188] also found that overlap can be valuable, however, they present their results rather abstractly so it is difficult to project them onto concrete scenarios – as far as we can tell our results are probably consistent.) Figure 5 attempts to illuminate what is really going on when surveys overlap. The Fourier space coverage of the redshift survey is limited at both high radial and transverse k by nonlinearities and the accompanying scale dependence of bias and stochasticity. The number density measurements for the photometric survey have similar coverage in the transverse direction but have drastically reduced coverage in the radial direction, set by the photo- z accuracy. Lensing is further limited in the radial direction because of the breadth of the lensing kernel, however, we expect that the signal can be predicted to significantly smaller transverse scales (the radial Fourier space coverage for lensing is not perfectly well-defined and has been drawn semi-arbitrarily in Fig. 5 – in any case, it is clearly significantly narrower than the photo- z band for relevant surveys). The take away point from Fig. 5 is that, even if you locate lensing and redshift surveys on the same patch of sky, the bulk of their modes, i.e., most of their constraining power, still do not really overlap. In some sense, the idea that it is even possible for these surveys to strongly overlap is an illusion. Redshift surveys get their constraining power from their fine radial resolution, which opens up a huge number of modes with substantial radial k component. Lensing surveys get their power from believing that, being directly sensitive to mass rather than a biased tracer, their signal is predictable down

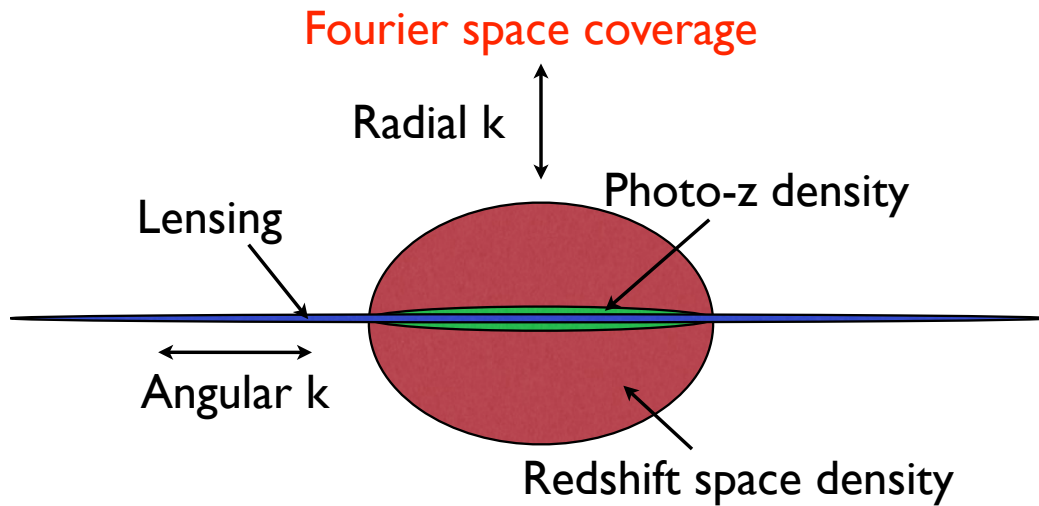


FIG. 5. Qualitative diagram of Fourier space coverage of elements of photometric and spectroscopic surveys. The red oval shows conceptually the Fourier space coverage of the redshift survey (the boundary of the red oval would correspond to $k \sim 0.1 - 0.2 \text{ hMpc}^{-1}$, the scale of breakdown of perturbation theory), the green oval shows the coverage of the photo- z density field, and the blue oval shows (even more qualitatively) the coverage of the lensing convergence field.

to much smaller scales, which opens up a large number of transverse modes (remember that the transverse direction is two dimensional, so Fig. 5 does not really do justice to the large number of modes present in the extended lensing coverage). This qualitative argument would certainly not be sufficient on its own, but it suggests that one is facing an uphill battle to find value in overlap. From this point of view the full Fisher matrix results should not be too surprising.

TABLE XI. DETF Figures of Merit (including marginalization over Σm_ν). See Table VIII for survey codes. All lines include a 5% H_0 constraint (which only matters for under-constrained cases).

Surveys	FoM	a_p	σ_{w_p}	σ_{Ω_k}
P	2	0.76	0.287	0.0085
P+BgB+BIB	12	0.51	0.095	0.0057
P+BgA0.1+BIB	22	0.60	0.076	0.0029
P+BgA0.2+BIB	25	0.60	0.075	0.0026
P+DES	38	0.71	0.032	0.0032
P+BgB+BIB+DES	71	0.71	0.028	0.0019
P+BgA0.1+BIB+DES	89	0.69	0.025	0.0019
P+BgA0.1+BIB+ebA0.1	32	0.60	0.058	0.0023
P+BgA0.2+BIB+ebA0.2	42	0.58	0.054	0.0020
P+BgA0.1+BIB+ebA0.1+DES	100	0.69	0.024	0.0018
P+hdB+BgB	13	0.52	0.094	0.0056
P+hdA0.1+BgA0.1	29	0.60	0.061	0.0026
P+hdA0.2+BgA0.2	45	0.57	0.045	0.0024
P+BBgB	23	0.52	0.070	0.0064
P+BBgB+BIB	27	0.53	0.063	0.0055
P+BBIB+BgB	17	0.54	0.082	0.0039
P+BBgB+BBIB	37	0.56	0.048	0.0036
P+BBgB+BBIB+DES	128	0.70	0.024	0.0013
P+BBgA0.1	104	0.67	0.029	0.0013
P+BBgA0.1+BBIB	117	0.67	0.029	0.0012
P+BBgA0.1+BBIB+DES	186	0.69	0.019	0.0012
P+BBgA0.2+BBIB	199	0.63	0.024	0.0010
P+BBgA0.2+BBIB+DES	327	0.67	0.015	0.0010
P+BB24gB+BB24IB	58	0.56	0.037	0.0029
P+BB24gA0.1+BB24IB	182	0.66	0.023	0.0011
P+BB24gA0.1+BB24IB+DES	258	0.68	0.017	0.0010
P+BB24gA0.2+BB24IB	318	0.62	0.018	0.0008
P+BB24gA0.2+BB24IB+DES	459	0.66	0.013	0.0008
P+BgB+BIB+euB	27	0.54	0.062	0.0052
P+BgA0.1+BIB+euA0.1	123	0.69	0.028	0.0012
P+BgA0.1+BIB+euA0.1+DES	183	0.71	0.019	0.0011
P+BgA0.2+BIB+euA0.2	228	0.65	0.021	0.0009
P+BgA0.2+BIB+euA0.2+DES	342	0.68	0.015	0.0009
P+BB24gA0.1+BB24IB+euA0.1	250	0.67	0.020	0.0009
P+BB24gA0.1+BB24IB+euA0.1+DES	320	0.68	0.016	0.0009
P+BB24gA0.2+BB24IB+euA0.2	468	0.63	0.015	0.0007
P+BB24gA0.2+BB24IB+euA0.2+DES	595	0.66	0.012	0.0007
P+LSST	134	0.72	0.019	0.0019
P+BgB+BIB+LSST	176	0.72	0.017	0.0013
P+BBgB+BBIB+LSST	230	0.71	0.017	0.0011
P+BBgA0.1+BBIB+LSST	300	0.70	0.014	0.0010
P+BBgA0.2+BBIB+LSST	518	0.69	0.011	0.0009
P+BB24gA0.1+BB24IB+LSST	391	0.69	0.013	0.0009
P+BB24gA0.2+BB24IB+LSST	708	0.68	0.010	0.0008
P+BB24gA0.1+BB24IB+euA0.1+LSST	467	0.70	0.012	0.0008
P+BB24gA0.2+BB24IB+euA0.2+LSST	877	0.68	0.009	0.0007
P+wfB+BgB	19	0.55	0.077	0.0054
P+wfA0.1+BgA0.1	69	0.68	0.038	0.0014
P+wfA0.2+BgA0.2	116	0.63	0.031	0.0012

TABLE XIII. Projections in the FoM parameter space. See Table VIII for survey codes.

	ω_m	ω_b	θ_s	a_p	w_p	w_0	w'	Ω_k	Σm_ν	n_s
value	0.141	0.0221	0.597		-1.00	-1.00	0.00	0	0.0600	0.961
<i>P</i>	0.011	0.00015	0.00095	0.64	0.29	0.66	1.6	0.0085	1.0	0.0050
<i>P</i> + <i>BgB</i> + <i>BlB</i>	0.0069	0.00015	0.00064	0.80	0.095	0.21	0.90	0.0057	0.66	0.0045
<i>P</i> + <i>BgA0.1</i> + <i>BlB</i>	0.0026	0.00014	0.00025	0.74	0.076	0.17	0.60	0.0029	0.18	0.0034
<i>P</i> + <i>BgA0.2</i> + <i>BlB</i>	0.0023	0.00013	0.00023	0.74	0.075	0.16	0.53	0.0026	0.15	0.0033
<i>P</i> + <i>DES</i>	0.0017	0.00014	0.00019	0.66	0.032	0.29	0.84	0.0032	0.063	0.0034
<i>P</i> + <i>BgB</i> + <i>BlB</i> + <i>DES</i>	0.0016	0.00014	0.00019	0.67	0.028	0.17	0.51	0.0019	0.054	0.0034
<i>P</i> + <i>BgA0.1</i> + <i>BlB</i> + <i>DES</i>	0.0016	0.00014	0.00018	0.68	0.025	0.15	0.45	0.0019	0.052	0.0033
<i>P</i> + <i>BgA0.1</i> + <i>BlB</i> + <i>ebA0.1</i>	0.0021	0.00014	0.00022	0.73	0.058	0.15	0.54	0.0023	0.13	0.0034
<i>P</i> + <i>BgA0.2</i> + <i>BlB</i> + <i>ebA0.2</i>	0.0019	0.00013	0.00021	0.75	0.054	0.12	0.44	0.0020	0.11	0.0033
<i>P</i> + <i>BgA0.1</i> + <i>BlB</i> + <i>ebA0.1</i> + <i>DES</i>	0.0016	0.00014	0.00018	0.68	0.024	0.14	0.42	0.0018	0.050	0.0033
<i>P</i> + <i>hdB</i> + <i>BgB</i>	0.0066	0.00015	0.00062	0.79	0.094	0.20	0.85	0.0056	0.64	0.0044
<i>P</i> + <i>hdA0.1</i> + <i>BgA0.1</i>	0.0021	0.00014	0.00022	0.73	0.061	0.16	0.57	0.0026	0.13	0.0034
<i>P</i> + <i>hdA0.2</i> + <i>BgA0.2</i>	0.0017	0.00013	0.00019	0.75	0.045	0.13	0.49	0.0024	0.086	0.0033
<i>P</i> + <i>BBgB</i>	0.0067	0.00015	0.00061	0.79	0.070	0.15	0.61	0.0064	0.64	0.0044
<i>P</i> + <i>BBgB</i> + <i>BlB</i>	0.0059	0.00015	0.00055	0.78	0.063	0.15	0.60	0.0055	0.57	0.0043
<i>P</i> + <i>BBlB</i> + <i>BgB</i>	0.0053	0.00015	0.00051	0.77	0.082	0.18	0.73	0.0039	0.52	0.0042
<i>P</i> + <i>BBgB</i> + <i>BBlB</i>	0.0042	0.00015	0.00041	0.76	0.048	0.14	0.56	0.0036	0.41	0.0040
<i>P</i> + <i>BBgB</i> + <i>BBlB</i> + <i>DES</i>	0.0016	0.00014	0.00018	0.67	0.024	0.11	0.33	0.0013	0.051	0.0033
<i>P</i> + <i>BBgA0.1</i>	0.0015	0.00013	0.00018	0.69	0.029	0.10	0.33	0.0013	0.058	0.0032
<i>P</i> + <i>BBgA0.1</i> + <i>BBlB</i>	0.0015	0.00013	0.00018	0.69	0.029	0.095	0.29	0.0012	0.058	0.0032
<i>P</i> + <i>BBgA0.1</i> + <i>BBlB</i> + <i>DES</i>	0.0014	0.00013	0.00018	0.68	0.019	0.092	0.28	0.0012	0.044	0.0031
<i>P</i> + <i>BBgA0.2</i> + <i>BBlB</i>	0.0012	0.00011	0.00017	0.71	0.024	0.065	0.21	0.00098	0.047	0.0030
<i>P</i> + <i>BBgA0.2</i> + <i>BBlB</i> + <i>DES</i>	0.0012	0.00011	0.00016	0.69	0.015	0.064	0.20	0.00097	0.038	0.0029
<i>P</i> + <i>BB24gB</i> + <i>BB24lB</i>	0.0035	0.00015	0.00035	0.76	0.037	0.12	0.46	0.0029	0.34	0.0039
<i>P</i> + <i>BB24gA0.1</i> + <i>BB24lB</i>	0.0014	0.00012	0.00018	0.70	0.023	0.075	0.24	0.0011	0.050	0.0031
<i>P</i> + <i>BB24gA0.1</i> + <i>BB24lB</i> + <i>DES</i>	0.0013	0.00012	0.00017	0.68	0.017	0.074	0.23	0.0010	0.041	0.0030
<i>P</i> + <i>BB24gA0.2</i> + <i>BB24lB</i>	0.0011	0.00010	0.00016	0.72	0.018	0.051	0.17	0.00083	0.040	0.0028
<i>P</i> + <i>BB24gA0.2</i> + <i>BB24lB</i> + <i>DES</i>	0.0010	0.00010	0.00016	0.70	0.013	0.051	0.16	0.00082	0.035	0.0027
<i>P</i> + <i>BgB</i> + <i>BlB</i> + <i>euB</i>	0.0057	0.00015	0.00053	0.77	0.062	0.15	0.61	0.0052	0.55	0.0042
<i>P</i> + <i>BgA0.1</i> + <i>BlB</i> + <i>euA0.1</i>	0.0014	0.00012	0.00018	0.68	0.028	0.099	0.29	0.0012	0.051	0.0032
<i>P</i> + <i>BgA0.1</i> + <i>BlB</i> + <i>euA0.1</i> + <i>DES</i>	0.0014	0.00012	0.00017	0.67	0.019	0.096	0.28	0.0011	0.042	0.0032
<i>P</i> + <i>BgA0.2</i> + <i>BlB</i> + <i>euA0.2</i>	0.0011	0.00010	0.00017	0.70	0.021	0.064	0.20	0.00091	0.041	0.0029
<i>P</i> + <i>BgA0.2</i> + <i>BlB</i> + <i>euA0.2</i> + <i>DES</i>	0.0011	0.00010	0.00016	0.68	0.015	0.064	0.19	0.00090	0.035	0.0029
<i>P</i> + <i>BB24gA0.1</i> + <i>BB24lB</i> + <i>euA0.1</i>	0.0012	0.00011	0.00017	0.69	0.020	0.066	0.20	0.00093	0.042	0.0030
<i>P</i> + <i>BB24gA0.1</i> + <i>BB24lB</i> + <i>euA0.1</i> + <i>DES</i>	0.0012	0.00011	0.00017	0.68	0.016	0.065	0.20	0.00092	0.038	0.0029
<i>P</i> + <i>BB24gA0.2</i> + <i>BB24lB</i> + <i>euA0.2</i>	0.00098	9.7e-05	0.00016	0.71	0.015	0.044	0.14	0.00070	0.034	0.0026
<i>P</i> + <i>BB24gA0.2</i> + <i>BB24lB</i> + <i>euA0.2</i> + <i>DES</i>	0.00095	9.6e-05	0.00016	0.70	0.012	0.044	0.14	0.00070	0.031	0.0025
<i>P</i> + <i>LSST</i>	0.0013	0.00013	0.00017	0.66	0.019	0.13	0.38	0.0019	0.035	0.0032
<i>P</i> + <i>BgB</i> + <i>BlB</i> + <i>LSST</i>	0.0013	0.00013	0.00017	0.66	0.017	0.11	0.33	0.0013	0.034	0.0032
<i>P</i> + <i>BBgB</i> + <i>BBlB</i> + <i>LSST</i>	0.0013	0.00013	0.00017	0.66	0.017	0.089	0.26	0.0011	0.033	0.0031
<i>P</i> + <i>BBgA0.1</i> + <i>BBlB</i> + <i>LSST</i>	0.0012	0.00012	0.00017	0.67	0.014	0.078	0.23	0.0010	0.032	0.0030
<i>P</i> + <i>BBgA0.2</i> + <i>BBlB</i> + <i>LSST</i>	0.0010	0.00010	0.00016	0.68	0.011	0.058	0.18	0.00088	0.029	0.0028
<i>P</i> + <i>BB24gA0.1</i> + <i>BB24lB</i> + <i>LSST</i>	0.0011	0.00011	0.00016	0.67	0.013	0.065	0.20	0.00090	0.031	0.0029
<i>P</i> + <i>BB24gA0.2</i> + <i>BB24lB</i> + <i>LSST</i>	0.00092	0.00010	0.00016	0.68	0.0096	0.048	0.15	0.00076	0.028	0.0026
<i>P</i> + <i>BB24gA0.1</i> + <i>BB24lB</i> + <i>euA0.1</i> + <i>LSST</i>	0.0010	0.00011	0.00016	0.67	0.012	0.059	0.18	0.00082	0.030	0.0028
<i>P</i> + <i>BB24gA0.2</i> + <i>BB24lB</i> + <i>euA0.2</i> + <i>LSST</i>	0.00086	9.6e-05	0.00015	0.68	0.0089	0.042	0.13	0.00066	0.026	0.0024
<i>P</i> + <i>wfB</i> + <i>BgB</i>	0.0060	0.00015	0.00056	0.77	0.077	0.18	0.68	0.0054	0.58	0.0043
<i>P</i> + <i>wfA0.1</i> + <i>BgA0.1</i>	0.0017	0.00014	0.00019	0.68	0.038	0.13	0.38	0.0014	0.072	0.0033
<i>P</i> + <i>wfA0.2</i> + <i>BgA0.2</i>	0.0014	0.00012	0.00018	0.72	0.031	0.085	0.28	0.0012	0.053	0.0031

TABLE XV. Projections for modified gravity parameters. See Table VIII for survey codes.

	ω_m	a_p	w_p	w_0	w'	Ω_k	Σm_ν	n_s	$\Delta\gamma$	G_9
value	0.14		-1.0	-1.0	0.0	0	0.060	0.96	0.0	1.0
$P + BgA0.1 + BlB$	0.0036	0.75	0.077	0.18	0.66	0.0037	0.30	0.0036	0.18	0.14
$P + BgA0.2 + BlB$	0.0035	0.75	0.075	0.18	0.63	0.0035	0.28	0.0034	0.10	0.094
$P + DES$	0.0029	0.65	0.046	0.35	1.0	0.0036	0.22	0.0035	0.16	0.063
$P + BgB + BlB + DES$	0.0023	0.66	0.038	0.18	0.51	0.0029	0.16	0.0035	0.13	0.044
$P + BgA0.1 + BlB + DES$	0.0023	0.66	0.033	0.17	0.49	0.0027	0.15	0.0034	0.067	0.037
$P + BgA0.1 + BlB + ebA0.1$	0.0029	0.73	0.061	0.17	0.60	0.0030	0.22	0.0034	0.10	0.074
$P + BgA0.2 + BlB + ebA0.2$	0.0028	0.73	0.057	0.16	0.57	0.0028	0.21	0.0033	0.070	0.060
$P + BgA0.1 + BlB + ebA0.1 + DES$	0.0022	0.66	0.032	0.16	0.45	0.0024	0.13	0.0034	0.062	0.034
$P + hdA0.1 + BgA0.1$	0.0032	0.73	0.070	0.18	0.63	0.0032	0.26	0.0035	0.093	0.082
$P + hdA0.2 + BgA0.2$	0.0030	0.73	0.060	0.17	0.60	0.0031	0.23	0.0034	0.061	0.066
$P + BBgB + BBBlB + DES$	0.0020	0.68	0.030	0.12	0.35	0.0018	0.13	0.0034	0.12	0.040
$P + BBgA0.1$	0.0023	0.70	0.035	0.12	0.37	0.0021	0.14	0.0033	0.041	0.036
$P + BBgA0.1 + BBBlB$	0.0022	0.71	0.034	0.11	0.34	0.0018	0.14	0.0032	0.039	0.033
$P + BBgA0.1 + BBBlB + DES$	0.0018	0.68	0.025	0.10	0.30	0.0016	0.10	0.0032	0.031	0.025
$P + BBgA0.2 + BBBlB$	0.0020	0.72	0.029	0.085	0.29	0.0016	0.13	0.0031	0.025	0.030
$P + BBgA0.2 + BBBlB + DES$	0.0016	0.68	0.021	0.078	0.24	0.0014	0.096	0.0031	0.022	0.024
$P + BB2gA0.1 + BB2lB$	0.0019	0.71	0.027	0.083	0.28	0.0015	0.11	0.0032	0.030	0.026
$P + BB2gA0.1 + BB2lB + DES$	0.0017	0.69	0.022	0.080	0.25	0.0014	0.090	0.0031	0.025	0.022
$P + BB2gA0.2 + BB2lB$	0.0016	0.73	0.023	0.066	0.23	0.0013	0.11	0.0029	0.019	0.024
$P + BB2gA0.2 + BB2lB + DES$	0.0014	0.69	0.018	0.062	0.19	0.0012	0.084	0.0029	0.017	0.020
$P + BgA0.1 + BlB + euA0.1$	0.0021	0.68	0.036	0.12	0.36	0.0018	0.13	0.0032	0.052	0.032
$P + BgA0.1 + BlB + euA0.1 + DES$	0.0018	0.66	0.027	0.11	0.33	0.0016	0.10	0.0032	0.043	0.025
$P + BgA0.2 + BlB + euA0.2$	0.0018	0.68	0.031	0.11	0.32	0.0015	0.12	0.0030	0.037	0.028
$P + BgA0.2 + BlB + euA0.2 + DES$	0.0015	0.65	0.023	0.099	0.28	0.0013	0.092	0.0030	0.033	0.023
$P + BB2gA0.1 + BB2lB + euA0.1$	0.0017	0.70	0.024	0.075	0.24	0.0014	0.095	0.0031	0.026	0.022
$P + BB2gA0.1 + BB2lB + euA0.1 + DES$	0.0016	0.69	0.020	0.073	0.22	0.0013	0.082	0.0031	0.023	0.019
$P + BB2gA0.2 + BB2lB + euA0.2$	0.0014	0.71	0.019	0.059	0.19	0.0011	0.085	0.0027	0.017	0.019
$P + BB2gA0.2 + BB2lB + euA0.2 + DES$	0.0012	0.69	0.016	0.056	0.17	0.00099	0.072	0.0027	0.016	0.017
$P + LSST$	0.0014	0.65	0.028	0.16	0.44	0.0020	0.070	0.0033	0.056	0.017
$P + BgB + BlB + LSST$	0.0014	0.65	0.022	0.13	0.35	0.0015	0.063	0.0033	0.050	0.015
$P + BBgB + BBBlB + LSST$	0.0014	0.65	0.021	0.095	0.27	0.0012	0.059	0.0033	0.046	0.013
$P + BBgA0.1 + BBBlB + LSST$	0.0013	0.66	0.017	0.085	0.24	0.0012	0.055	0.0032	0.024	0.012
$P + BBgA0.2 + BBBlB + LSST$	0.0011	0.66	0.014	0.069	0.20	0.0010	0.052	0.0030	0.018	0.011
$P + BB2gA0.1 + BB2lB + LSST$	0.0012	0.66	0.016	0.070	0.20	0.0010	0.053	0.0031	0.020	0.011
$P + BB2gA0.2 + BB2lB + LSST$	0.0010	0.66	0.013	0.056	0.16	0.00089	0.049	0.0029	0.014	0.011
$P + BB2gA0.1 + BB2lB + euA0.1 + LSST$	0.0011	0.66	0.015	0.065	0.19	0.00096	0.051	0.0030	0.018	0.011
$P + BB2gA0.2 + BB2lB + euA0.2 + LSST$	0.00095	0.66	0.012	0.051	0.15	0.00078	0.046	0.0027	0.013	0.010
$P + wfA0.1 + BgA0.1$	0.0026	0.68	0.049	0.15	0.46	0.0023	0.19	0.0034	0.072	0.049
$P + wfA0.2 + BgA0.2$	0.0024	0.69	0.045	0.14	0.41	0.0020	0.17	0.0032	0.050	0.042
$P + BgB + BlA + l1D$	0.0046	0.79	0.083	0.19	0.79	0.0031	0.42	0.0038	1.5	0.10
$P + BgA0.1 + BlA + l1D$	0.0032	0.76	0.073	0.16	0.59	0.0027	0.26	0.0035	0.066	0.062
$P + BgA0.2 + BlA + l1D$	0.0031	0.75	0.065	0.16	0.56	0.0026	0.24	0.0034	0.049	0.054
$P + BBgB + BBBlA + l1D$	0.0025	0.73	0.039	0.12	0.43	0.0019	0.21	0.0034	1.5	0.053
$P + BBgA0.1 + BBBlA + l1D$	0.0019	0.71	0.033	0.097	0.32	0.0015	0.12	0.0030	0.031	0.025
$P + BBgA0.2 + BBBlA + l1D$	0.0017	0.73	0.028	0.080	0.28	0.0013	0.12	0.0028	0.021	0.023
$P + BB2gB + BB2lA + l1D$	0.0021	0.74	0.031	0.096	0.34	0.0016	0.17	0.0033	1.5	0.044
$P + BB2gA0.1 + BB2lA + l1D$	0.0016	0.72	0.026	0.076	0.25	0.0012	0.10	0.0028	0.024	0.020
$P + BB2gA0.2 + BB2lA + l1D$	0.0014	0.73	0.022	0.063	0.22	0.0011	0.094	0.0025	0.017	0.018
$P + BB2gA0.2 + BB2lA + l1D + euA0.2$	0.0012	0.71	0.018	0.056	0.19	0.00091	0.076	0.0023	0.015	0.016
$P + BB2gA0.2 + BB2lA + l1D + LSST$	0.00092	0.66	0.012	0.053	0.15	0.00082	0.043	0.0024	0.014	0.0091
$P + BB2gA0.2 + BB2lA + l1D + euA0.2 + LSST$	0.00086	0.66	0.012	0.049	0.14	0.00072	0.041	0.0023	0.013	0.0087

TABLE XVII. Projections including running of the spectral index. See Table VIII for survey codes.

	ω_m	ω_b	θ_s	Σm_ν	$\log_{10}(A)$	n_s	α_s
value	0.141	0.0221	0.597	0.0600	-8.66	0.961	0.00
P	0.0037	0.00017	0.00036	0.35	0.0043	0.0038	0.0054
$P + BgB + BlB$	0.00074	0.00017	0.00014	0.10	0.0042	0.0038	0.0054
$P + BgA0.1 + BlB$	0.00070	0.00015	0.00014	0.069	0.0042	0.0031	0.0053
$P + BgA0.2 + BlB$	0.00072	0.00013	0.00015	0.046	0.0041	0.0028	0.0050
$P + DES$	0.0013	0.00014	0.00017	0.041	0.0041	0.0032	0.0049
$P + BgB + BlB + DES$	0.00070	0.00013	0.00014	0.030	0.0041	0.0027	0.0049
$P + BgA0.1 + BlB + DES$	0.00068	0.00013	0.00014	0.029	0.0041	0.0027	0.0049
$P + BgA0.1 + BlB + ebA0.1$	0.00064	0.00014	0.00014	0.053	0.0041	0.0029	0.0053
$P + BgA0.2 + BlB + ebA0.2$	0.00065	0.00013	0.00014	0.036	0.0040	0.0027	0.0049
$P + BgA0.1 + BlB + ebA0.1 + DES$	0.00062	0.00013	0.00014	0.028	0.0040	0.0026	0.0048
$P + hdB + BgB$	0.00074	0.00017	0.00014	0.10	0.0042	0.0038	0.0054
$P + hdA0.1 + BgA0.1$	0.00069	0.00015	0.00014	0.061	0.0041	0.0030	0.0053
$P + hdA0.2 + BgA0.2$	0.00069	0.00013	0.00014	0.039	0.0040	0.0027	0.0050
$P + BBgB$	0.00056	0.00017	0.00014	0.090	0.0042	0.0038	0.0054
$P + BBgB + BlB$	0.00056	0.00017	0.00014	0.090	0.0042	0.0038	0.0054
$P + BBIB + BgB$	0.00073	0.00017	0.00014	0.099	0.0042	0.0038	0.0054
$P + BBgB + BBIB$	0.00056	0.00017	0.00014	0.090	0.0042	0.0038	0.0054
$P + BBgB + BBIB + DES$	0.00047	0.00013	0.00014	0.027	0.0040	0.0025	0.0049
$P + BBgA0.1$	0.00045	0.00013	0.00014	0.025	0.0040	0.0024	0.0051
$P + BBgA0.1 + BBIB$	0.00045	0.00013	0.00014	0.025	0.0040	0.0024	0.0051
$P + BBgA0.1 + BBIB + DES$	0.00044	0.00013	0.00014	0.022	0.0040	0.0024	0.0046
$P + BBgA0.2 + BBIB$	0.00043	0.00011	0.00014	0.017	0.0037	0.0022	0.0040
$P + BBgA0.2 + BBIB + DES$	0.00043	0.00011	0.00014	0.017	0.0036	0.0022	0.0038
$P + BB2gB + BB2IB$	0.00053	0.00016	0.00014	0.088	0.0042	0.0037	0.0054
$P + BB2gA0.1 + BB2IB$	0.00039	0.00013	0.00014	0.021	0.0040	0.0023	0.0050
$P + BB2gA0.1 + BB2IB + DES$	0.00039	0.00012	0.00013	0.020	0.0040	0.0023	0.0045
$P + BB2gA0.2 + BB2IB$	0.00037	0.00010	0.00014	0.015	0.0036	0.0021	0.0036
$P + BB2gA0.2 + BB2IB + DES$	0.00037	0.00010	0.00014	0.015	0.0035	0.0021	0.0035
$P + BgB + BlB + euB$	0.00055	0.00017	0.00014	0.090	0.0042	0.0038	0.0054
$P + BgA0.1 + BlB + euA0.1$	0.00044	0.00013	0.00014	0.022	0.0040	0.0024	0.0050
$P + BgA0.1 + BlB + euA0.1 + DES$	0.00044	0.00012	0.00014	0.020	0.0040	0.0023	0.0046
$P + BgA0.2 + BlB + euA0.2$	0.00043	0.00011	0.00014	0.016	0.0037	0.0022	0.0037
$P + BgA0.2 + BlB + euA0.2 + DES$	0.00042	0.00011	0.00014	0.015	0.0035	0.0022	0.0036
$P + BB2gA0.1 + BB2IB + euA0.1$	0.00037	0.00013	0.00013	0.018	0.0039	0.0022	0.0047
$P + BB2gA0.1 + BB2IB + euA0.1 + DES$	0.00037	0.00012	0.00013	0.018	0.0039	0.0022	0.0043
$P + BB2gA0.2 + BB2IB + euA0.2$	0.00034	$9.9e - 05$	0.00013	0.014	0.0035	0.0019	0.0031
$P + BB2gA0.2 + BB2IB + euA0.2 + DES$	0.00034	$9.9e - 05$	0.00013	0.014	0.0034	0.0019	0.0030
$P + LSST$	0.00084	0.00012	0.00015	0.023	0.0039	0.0030	0.0038
$P + BgB + BlB + LSST$	0.00062	0.00012	0.00014	0.020	0.0039	0.0025	0.0038
$P + BBgB + BBIB + LSST$	0.00045	0.00012	0.00013	0.018	0.0038	0.0023	0.0037
$P + BBgA0.1 + BBIB + LSST$	0.00043	0.00012	0.00013	0.018	0.0038	0.0022	0.0036
$P + BBgA0.2 + BBIB + LSST$	0.00042	0.00011	0.00014	0.015	0.0033	0.0022	0.0033
$P + BB2gA0.1 + BB2IB + LSST$	0.00039	0.00012	0.00013	0.017	0.0038	0.0021	0.0035
$P + BB2gA0.2 + BB2IB + LSST$	0.00037	0.00010	0.00013	0.014	0.0031	0.0020	0.0030
$P + BB2gA0.1 + BB2IB + euA0.1 + LSST$	0.00036	0.00011	0.00013	0.016	0.0037	0.0020	0.0034
$P + BB2gA0.2 + BB2IB + euA0.2 + LSST$	0.00034	$9.9e - 05$	0.00013	0.012	0.0029	0.0019	0.0028
$P + wfB + BgB$	0.00065	0.00017	0.00014	0.096	0.0042	0.0038	0.0054
$P + wfA0.1 + BgA0.1$	0.00058	0.00014	0.00014	0.037	0.0041	0.0027	0.0053
$P + wfA0.2 + BgA0.2$	0.00057	0.00012	0.00014	0.021	0.0039	0.0025	0.0045
$P + BgB + BlA + l1D$	0.00067	0.00011	0.00014	0.068	0.0041	0.0033	0.0038
$P + BgA0.1 + BlA + l1D$	0.00065	0.00011	0.00014	0.056	0.0040	0.0030	0.0034
$P + BgA0.2 + BlA + l1D$	0.00066	0.00011	0.00014	0.043	0.0039	0.0027	0.0031
$P + BBgB + BBIA + l1D$	0.00041	0.00010	0.00014	0.047	0.0039	0.0029	0.0027
$P + BBgA0.1 + BBIA + l1D$	0.00040	0.00010	0.00014	0.023	0.0036	0.0023	0.0021
$P + BBgA0.2 + BBIA + l1D$	0.00038	0.00010	0.00014	0.017	0.0036	0.0022	0.0020
$P + BB2gB + BB2IA + l1D$	0.00036	0.00010	0.00014	0.040	0.0038	0.0028	0.0023
$P + BB2gA0.1 + BB2IA + l1D$	0.00035	0.00010	0.00014	0.019	0.0036	0.0022	0.0018
$P + BB2gA0.2 + BB2IA + l1D$	0.00034	$9.8e - 05$	0.00014	0.015	0.0035	0.0020	0.0017
$P + BB2gA0.2 + BB2IA + l1D + euA0.2$	0.00032	$9.6e - 05$	0.00013	0.014	0.0034	0.0019	0.0016
$P + BB2gA0.2 + BB2IA + l1D + LSST$	0.00034	$9.8e - 05$	0.00013	0.012	0.0026	0.0019	0.0016
$P + BB2gA0.2 + BB2IA + l1D + euA0.2 + LSST$	0.00032	$9.5e - 05$	0.00013	0.011	0.0025	0.0018	0.0016

TABLE XIX. Estimated constraints on f_{NL} .

Survey	$\sigma_{f_{\text{NL}}}$
BOSS	23
BOSS+eBOSS	11
DESI	3.8
BOSS+Euclid	6.7

TABLE XXI. Projections including N_ν . See Table VIII for survey codes.

	ω_m	ω_b	θ_s	Σm_ν	$N_{\nu,l}$	$\log_{10}(A)$	n_s
value	0.141	0.0221	0.597	0.0600	3.05	-8.66	0.961
P	0.0050	0.00023	0.00042	0.35	0.18	0.0049	0.0082
$P + BgB + BlB$	0.0033	0.00023	0.00026	0.12	0.18	0.0049	0.0081
$P + BgA0.1 + BlB$	0.0031	0.00020	0.00025	0.086	0.18	0.0048	0.0073
$P + BgA0.2 + BlB$	0.0025	0.00019	0.00022	0.061	0.15	0.0045	0.0061
$P + DES$	0.0020	0.00019	0.00020	0.048	0.12	0.0038	0.0059
$P + BgB + BlB + DES$	0.0019	0.00016	0.00020	0.045	0.11	0.0037	0.0048
$P + BgA0.1 + BlB + DES$	0.0019	0.00016	0.00019	0.043	0.11	0.0037	0.0048
$P + BgA0.1 + BlB + ebA0.1$	0.0029	0.00019	0.00024	0.068	0.17	0.0048	0.0068
$P + BgA0.2 + BlB + ebA0.2$	0.0022	0.00018	0.00020	0.048	0.13	0.0044	0.0055
$P + BgA0.1 + BlB + ebA0.1 + DES$	0.0018	0.00015	0.00019	0.041	0.11	0.0037	0.0046
$P + hdB + BgB$	0.0033	0.00023	0.00026	0.12	0.18	0.0049	0.0081
$P + hdA0.1 + BgA0.1$	0.0030	0.00020	0.00025	0.078	0.17	0.0048	0.0071
$P + hdA0.2 + BgA0.2$	0.0023	0.00018	0.00021	0.053	0.14	0.0045	0.0058
$P + BBgB$	0.0032	0.00023	0.00026	0.11	0.18	0.0049	0.0081
$P + BBgB + BlB$	0.0032	0.00023	0.00026	0.11	0.18	0.0049	0.0081
$P + BBBlB + BgB$	0.0033	0.00023	0.00026	0.12	0.18	0.0049	0.0081
$P + BBgB + BBBlB$	0.0032	0.00023	0.00026	0.11	0.18	0.0049	0.0081
$P + BBgB + BBBlB + DES$	0.0019	0.00015	0.00019	0.044	0.11	0.0037	0.0046
$P + BBgA0.1$	0.0022	0.00016	0.00020	0.036	0.13	0.0046	0.0048
$P + BBgA0.1 + BBBlB$	0.0022	0.00016	0.00020	0.036	0.13	0.0046	0.0048
$P + BBgA0.1 + BBBlB + DES$	0.0015	0.00014	0.00018	0.029	0.086	0.0036	0.0036
$P + BBgA0.2 + BBBlB$	0.0014	0.00014	0.00017	0.024	0.084	0.0042	0.0031
$P + BBgA0.2 + BBBlB + DES$	0.0012	0.00013	0.00017	0.021	0.070	0.0035	0.0027
$P + BB24gB + BB24lB$	0.0032	0.00023	0.00026	0.11	0.18	0.0049	0.0081
$P + BB24gA0.1 + BB24lB$	0.0020	0.00015	0.00019	0.031	0.11	0.0045	0.0041
$P + BB24gA0.1 + BB24lB + DES$	0.0014	0.00013	0.00017	0.026	0.079	0.0035	0.0032
$P + BB24gA0.2 + BB24lB$	0.0013	0.00014	0.00017	0.022	0.074	0.0041	0.0025
$P + BB24gA0.2 + BB24lB + DES$	0.0011	0.00013	0.00016	0.019	0.063	0.0035	0.0023
$P + BgB + BlB + euB$	0.0032	0.00023	0.00026	0.11	0.18	0.0049	0.0081
$P + BgA0.1 + BlB + euA0.1$	0.0021	0.00015	0.00020	0.031	0.12	0.0045	0.0044
$P + BgA0.1 + BlB + euA0.1 + DES$	0.0014	0.00013	0.00017	0.026	0.081	0.0035	0.0033
$P + BgA0.2 + BlB + euA0.2$	0.0013	0.00014	0.00017	0.022	0.077	0.0041	0.0028
$P + BgA0.2 + BlB + euA0.2 + DES$	0.0011	0.00013	0.00016	0.019	0.065	0.0035	0.0025
$P + BB24gA0.1 + BB24lB + euA0.1$	0.0017	0.00014	0.00018	0.026	0.097	0.0044	0.0035
$P + BB24gA0.1 + BB24lB + euA0.1 + DES$	0.0013	0.00013	0.00017	0.022	0.072	0.0035	0.0028
$P + BB24gA0.2 + BB24lB + euA0.2$	0.0012	0.00013	0.00016	0.019	0.065	0.0040	0.0021
$P + BB24gA0.2 + BB24lB + euA0.2 + DES$	0.0010	0.00012	0.00016	0.017	0.057	0.0034	0.0019
$P + LSST$	0.00096	0.00014	0.00016	0.020	0.063	0.0031	0.0038
$P + BgB + BlB + LSST$	0.00094	0.00012	0.00016	0.018	0.055	0.0030	0.0029
$P + BBgB + BBBlB + LSST$	0.00093	0.00012	0.00016	0.017	0.051	0.0030	0.0023
$P + BBgA0.1 + BBBlB + LSST$	0.00090	0.00012	0.00016	0.016	0.050	0.0029	0.0023
$P + BBgA0.2 + BBBlB + LSST$	0.00086	0.00012	0.00016	0.014	0.049	0.0027	0.0021
$P + BB24gA0.1 + BB24lB + LSST$	0.00089	0.00011	0.00016	0.015	0.049	0.0028	0.0021
$P + BB24gA0.2 + BB24lB + LSST$	0.00083	0.00011	0.00016	0.013	0.046	0.0025	0.0019
$P + BB24gA0.1 + BB24lB + euA0.1 + LSST$	0.00086	0.00011	0.00016	0.014	0.047	0.0027	0.0020
$P + BB24gA0.2 + BB24lB + euA0.2 + LSST$	0.00079	0.00011	0.00015	0.012	0.043	0.0024	0.0017
$P + wfB + BgB$	0.0033	0.00023	0.00026	0.12	0.18	0.0049	0.0081
$P + wfA0.1 + BgA0.1$	0.0026	0.00018	0.00022	0.050	0.15	0.0047	0.0060
$P + wfA0.2 + BgA0.2$	0.0017	0.00016	0.00018	0.030	0.11	0.0043	0.0042
$P + BgB + BlA + l1D$	0.0026	0.00021	0.00023	0.11	0.15	0.0042	0.0073
$P + BgA0.1 + BlA + l1D$	0.0022	0.00019	0.00021	0.083	0.13	0.0042	0.0059
$P + BgA0.2 + BlA + l1D$	0.0019	0.00017	0.00019	0.059	0.11	0.0041	0.0047
$P + BBgB + BBBlA + l1D$	0.0020	0.00018	0.00020	0.082	0.11	0.0041	0.0056
$P + BBgA0.1 + BBBlA + l1D$	0.0013	0.00013	0.00017	0.031	0.070	0.0039	0.0025
$P + BBgA0.2 + BBBlA + l1D$	0.0012	0.00013	0.00016	0.022	0.063	0.0038	0.0021
$P + BB24gB + BB24lA + l1D$	0.0018	0.00017	0.00018	0.071	0.099	0.0040	0.0048
$P + BB24gA0.1 + BB24lA + l1D$	0.0012	0.00013	0.00016	0.026	0.062	0.0038	0.0020
$P + BB24gA0.2 + BB24lA + l1D$	0.0011	0.00013	0.00016	0.019	0.057	0.0037	0.0017
$P + BB24gA0.2 + BB24lA + l1D + euA0.2$	0.0010	0.00012	0.00016	0.017	0.054	0.0036	0.0016
$P + BB24gA0.2 + BB24lA + l1D + LSST$	0.00081	0.00011	0.00015	0.013	0.043	0.0025	0.0015
$P + BB24gA0.2 + BB24lA + l1D + euA0.2 + LSST$	0.00078	0.00011	0.00015	0.011	0.041	0.0024	0.0014

TABLE XXIII. Original DETF Figures of Merit, i.e., *not* marginalized over Σm_ν . See Table VIII for survey codes.

Surveys	FoM	a_p	σ_{w_p}	σ_{Ω_k}
P+BgB+BIB	37	0.65	0.055	0.0026
P+BgA0.1+BIB	53	0.62	0.040	0.0025
P+BgA0.1+BIB+ebA0.1	80	0.65	0.032	0.0020
P+DES	45	0.73	0.032	0.0024
P+BgB+BIB+DES	85	0.72	0.028	0.0014
P+BgA0.1+BIB+DES	112	0.69	0.024	0.0014
P+BgA0.1+BIB+ebA0.1	80	0.65	0.032	0.0020
P+BgA0.1+BIB+ebA0.2	106	0.66	0.026	0.0019
P+BgA0.1+BIB+ebA0.1+DES	137	0.70	0.021	0.0013
P+BBgB	128	0.71	0.023	0.0013
P+BBgB+BIB	134	0.72	0.023	0.0012
P+BBIB+BgB	77	0.77	0.037	0.0013
P+BBgB+BBIB	166	0.73	0.023	0.0010
P+BBgA0.1	291	0.73	0.016	0.0010
P+BBgA0.1+BBIB	342	0.75	0.015	0.0008
P+BBgA0.1+DES	360	0.74	0.013	0.0009
P+BBgA0.1+BBIB+DES	410	0.75	0.013	0.0008
P+BBgA0.2+BBIB	756	0.74	0.011	0.0007
P+BBgA0.2+BBIB+DES	948	0.74	0.009	0.0007
P+BB24gB+BB24IB	252	0.72	0.019	0.0009
P+BB24gA0.1+BB24IB	557	0.75	0.012	0.0007
P+BB24gA0.1+BB24IB+DES	647	0.75	0.010	0.0006
P+BB24gA0.2+BB24IB	1194	0.73	0.009	0.0006
P+BB24gA0.2+BB24IB+DES	1454	0.74	0.007	0.0005
P+BgB+BIB+euB	152	0.75	0.022	0.0010
P+BgA0.1+BIB+euA0.1	366	0.77	0.014	0.0008
P+BgA0.1+BIB+euA0.1+DES	448	0.77	0.012	0.0007
P+BgA0.2+BIB+euA0.2	844	0.76	0.010	0.0006
P+BgA0.2+BIB+euA0.2+DES	1080	0.76	0.008	0.0006
P+BB24gA0.1+BB24IB+euA0.1	787	0.76	0.010	0.0006
P+BB24gA0.1+BB24IB+euA0.1+DES	908	0.76	0.009	0.0005
P+BB24gA0.2+BB24IB+euA0.2	1695	0.74	0.008	0.0005
P+BB24gA0.2+BB24IB+euA0.2+DES	2025	0.75	0.006	0.0005
P+LSST	221	0.76	0.013	0.0015
P+BgB+BIB+LSST	291	0.76	0.012	0.0010
P+BB24gA0.1+BB24IB+LSST	934	0.75	0.008	0.0006
P+BB24gA0.2+BB24IB+LSST	2165	0.74	0.005	0.0005
P+BB24gA0.1+BB24IB+euA0.1+LSST	1262	0.76	0.007	0.0005
P+BB24gA0.2+BB24IB+euA0.2+LSST	3124	0.76	0.004	0.0004

TABLE XXV. Original DETF Figures of Merit including Planck CMB *from FoMSWG* (indicated by P3 – normally we compute our own Planck Fisher matrix, because FoMSWG did not include neutrinos). WL3 stands for the FoMSWG Stage III weak lensing Fisher matrix. See Table VIII for other survey codes.

Surveys	FoM	a_p	σ_{w_p}	σ_{Ω_k}
P3+BgB+BIB	31	0.62	0.057	0.0030
P3+BBgB+BBIB	160	0.72	0.023	0.0010
P3+BBgA0.1+BBIB	265	0.73	0.018	0.0009
P3+DES	35	0.73	0.035	0.0031
P3+WL3	15	0.67	0.068	0.0029
P3+BBgA0.1+BBIB+DES	382	0.74	0.013	0.0008
P3+BBgA0.1+BBIB+WL3	287	0.74	0.018	0.0008

TABLE XXVII. FoM (with neutrinos, i.e., like Table XIII) for overlapping vs. non-overlapping DESI and LSST (to be clear, DESI is always 14000 sq. deg., and LSST always 20000, but in the overlapping case the 14000 sq. deg. DESI area is assumed be covered by LSST, while in the non-overlapping case it is not). See Table VIII for other survey codes.

Surveys	Δz	FoM	a_p	σ_{w_p}	σ_{Ω_k}
P+BBgA0.1	0.2	109	0.66	0.029	0.0013
P+LSST	0.2	134	0.72	0.019	0.0019
P+BBgA0.1+LSST-no overlap	0.2	288	0.71	0.014	0.0011
P+BBgA0.1+LSST-overlap	0.2	308	0.71	0.014	0.0010
P+BBgA0.1	0.1	105	0.66	0.029	0.0014
P+LSST	0.1	162	0.73	0.018	0.0017
P+BBgA0.1+LSST-no overlap	0.1	314	0.71	0.014	0.0010
P+BBgA0.1+LSST-overlap	0.1	329	0.71	0.013	0.0010